Transferrin Receptor Is a Specific Ferroptosis Marker

Huizhong Feng[1], **Kenji Schorpp**[2], **Jenny Jin**[1], **Carrie E. Yozwiak**[3], **Benjamin G. Hoffstrom**[4], **Aubrianna M. Decker**[1], **Presha Rajbhandari**[1], **Michael E. Stokes**[1], **Hannah G. Bender**[1], **Joleen M. Csuka**[1], **Pavan S. Upadhyayula**[5], **Peter Canoll**[6,7], **Koji Uchida**[8], **Rajesh K. Soni**[9], **Kamyar Hadian**[2], **Brent R. Stockwell**[1,3,7,10,*]

[1]Department of Biological Sciences, Columbia University, Northwest Corner Building, 12th Floor, MC 4846, 550 West 120th Street, New York, NY 10027, USA

[2]HelmholtzZentrum München, German Research Center for Environmental Health (GmbH), Assay Development and Screening Platform, Institute for Molecular Toxicology and Pharmacology, Ingolstädter Landstr. 1, 85764 Neuherberg, Germany

[3]Department of Chemistry, Columbia University, Northwest Corner Building, 12th Floor, MC 4846, 550 West 120th Street, New York, NY 10027, USA

[4]Antibody Technology Resource, Fred Hutchinson Cancer Research Center, 1100 Fairview Ave. N, Seattle, WA 98109, USA

[5]Department of Neurological Surgery, Vagelos College of Physicians and Surgeons, Columbia University Irving Medical Center, New York, NY 10032, USA

[6]Department of Pathology and Cell Biology, Vagelos College of Physicians and Surgeons, Columbia University Irving Medical Center, 1130 St. Nicholas Ave., Room 1001, New York, NY 10032, USA

[7]Herbert Irving Comprehensive Cancer Center, Columbia University Irving Medical Center, New York, NY 10032, USA

[8]Graduate School of Agricultural and Life Sciences, The University of Tokyo, Tokyo 113-8657, Japan

[9]Proteomics and Macromolecular Crystallography Shared Resource, Herbert Irving Comprehensive Cancer Center, Columbia University Irving Medical Center, New York, NY 10032, USA

[10]Lead Contact

*Correspondence: bstockwell@columbia.edu.

SUPPLEMENTAL INFORMATION

Supplemental Information can be found online at https://doi.org/10.1016/j.celrep.2020.02.049.

SUMMARY

Ferroptosis is a type of regulated cell death driven by the iron-dependent accumulation of oxidized polyunsaturated fatty acid-containing phospholipids. There is no reliable way to selectively stain ferroptotic cells in tissue sections to characterize the extent of ferroptosis in animal models or patient samples. We address this gap by immunizing mice with membranes from lymphoma cells treated with the ferroptosis inducer piperazine erastin and screening ~4,750 of the resulting monoclonal antibodies generated for their ability to selectively detect cells undergoing ferroptosis. We find that one antibody, 3F3 ferroptotic membrane antibody (3F3-FMA), is effective as a selective ferroptosis-staining reagent. The antigen of 3F3-FMA is identified as the human transferrin receptor 1 protein (TfR1). We validate this finding with several additional anti-TfR1 antibodies and compare them to other potential ferroptosis-detecting reagents. We find that anti-TfR1 and anti-malondialdehyde adduct antibodies are effective at staining ferroptotic tumor cells in multiple cell culture and tissue contexts.

Graphical Abstract
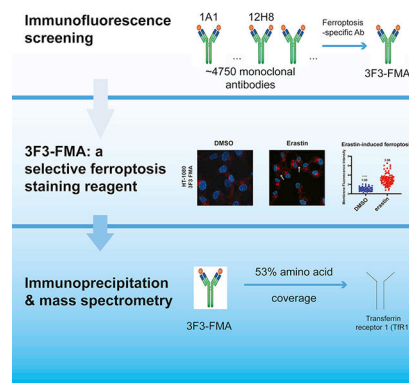
In Brief

Feng et al. find that 3F3-FMA detects ferroptotic cells by screening ~4,750 antibodies generated from mice immunized with membranes from DLBCL cells undergoing ferroptosis. The antigen of 3F3-FMA is the TfR1 protein. 3F3-FMA and other anti-TfR1 antibodies can be used to detect ferroptosis in cell culture and in cancer models.

INTRODUCTION

Ferroptosis is a regulated form of cell death that involves the accumulation of lethal phospholipid peroxides and is suppressed by iron chelators and lipophilic antioxidants (Stockwell et al., 2017). Ferroptosis is often characterized by the loss of activity of glutathione peroxidase 4 (GPX4), which is the major protein in animals that can reduce lipid hydroperoxides in a membrane phospholipid context (Yang et al., 2014).

Ferroptosis induction has been suggested to have potential as an anti-cancer therapeutic strategy. Unlike apoptosis, which many cancer cells can evade, ferroptosis is lethal to many tumor cells that have become dependent on the suppression of ferroptosis for their survival,

including some of the most drug-resistant and aggressive cancer cells, such as persister cells, and cells that have undergone epithelial-mesenchymal transition (EMT) (Hangauer et al., 2017; Viswanathan et al., 2017). Thus, triggering ferroptosis may open up new therapeutic avenues for treating drug-resistant cancers (Hangauer et al., 2017).

Ferroptosis is implicated in numerous human diseases and pathologies. It has been suggested that ferroptosis plays a role in the progression of degenerative diseases of the kidney, heart, liver, and brain (Feng and Stockwell, 2018); stroke, Alzheimer disease, Huntington disease (HD), and Parkinson disease are among the candidates for neurodegenerative diseases that may involve ferroptosis (Weiland et al., 2019).

To identify the extent to which ferroptosis occurs in specific pathological and physiological contexts, it is useful to identify reagents that selectively label cells undergoing ferroptosis. Three hallmarks of ferroptosis, oxidation of polyunsaturated fatty acid-containing phospholipids (PUFA-PLs), accumulation of redox-active iron, and loss of lipid peroxide repair capacity, have been used as criteria to measure the extent to which ferroptosis occurs (Dixon and Stockwell, 2019). First, the fluorescent probes C11-BODIPY and Liperfluo are used as indicators of lipid peroxidation. BODIPY-C11 indicates the production of reactive oxygen species (ROS) in a lipophilic environment through a change in the fluorescence of the probe; it is sensitive to reactive species formed from hydroperoxides, but not to hydroperoxides themselves (Drummen et al., 2002). Liperfluo directly reacts with lipid hydroperoxides to form fluorescent Liperfluo-OX, which can be detected at long wavelengths (Yamanaka et al., 2012). Second, several probes can quantitatively determine the relative abundance and the ratio of ferrous (Fe^{2+}) to ferric (Fe^{3+}) iron. Third, the loss of lipid peroxide repair is commonly determined by the abundance or enzymatic activity of GPX4, or its key co-substrate, glutathione. However, these experiments are technically challenging, are limited to biochemical assays, and cannot be used in fixed tissue sections. Thus, there is no robust method available to analyze tissue sections from human patients and animal models to determine the extent to which cells are specifically undergoing ferroptosis.

A ferroptosis-specific antibody would facilitate examining the consequences of ferroptosis in a variety of contexts, including in tissue sections, as well as cells in culture. Several antigens have been proposed as potential indicators of ferroptosis. For example, *PTGS2* mRNA, encoding cyclooxygenase-2 (COX-2), was the most upregulated gene in BJeLR cells upon treatment with either erastin or RSL3 in a survey of 83 oxidative stress genes (Yang et al., 2014). *CHAC1* mRNA (cation transport regulator homolog 1), an endoplasmic reticulum (ER) stress-response gene, was found to be upregulated upon the inhibition of system x_c^-, the transmembrane cystine-glutamate antiporter, which imports cystine into cells (Dixon et al., 2014). qRT-PCR is used to measure the mRNA level of *PTGS2* and *CHAC1* in cells. However, detecting ferroptosis using antibodies against the proteins encoded by these genes has proved challenging; moreover, *CHAC1* mRNA is primarily upregulated by system x_c^- inhibitors, but not by other ferroptosis inducers, and *PTGS2* is upregulated in specific contexts.

Acyl-coenzyme A (CoA) synthetase long-chain family member 4 (ACSL4) was found to be required for ferroptotic cell death (Dixon et al., 2015; Doll et al., 2017; Yuan et al., 2016).

The expression of ACSL4 was downregulated in ferroptosis-resistant cells compared to ferroptosis-sensitive cells (Yuan et al., 2016). However, it is not established that the expression level of ACSL4 changes for ferroptosis-sensitive cells undergoing ferroptosis (Müller et al., 2017).

MDA (malondialdehyde) and 4-HNE (4-hydroxynonenal) are aldehyde secondary products of lipid peroxidation. Antibodies against these species and their protein adducts are candidate ferroptosis markers. The 1F83 anti-MDA adduct antibody was raised to target malondialdehyde-modified proteins (Yamada et al., 2001). It has been used as a ferroptosis marker in tissue sections from a mouse lymphoma xenograft model (Zhang et al., 2019). However, MDA adducts are also markers of oxidative stress and may not be specific for ferroptosis compared to other oxidative stress contexts. Therefore, additional specific antibodies that differentiate between ferroptosis and oxidative stress are needed.

Here, we report the production of an untargeted pool of monoclonal antibodies from the spleens of mice that were challenged with the membrane fractions of cells induced to undergo ferroptosis with piperazine erastin (PE), an erastin analog and system x_c^- inhibitor. After screening ~4,750 monoclonal antibodies by flow cytometry, 672 antibodies were selected as candidate staining reagents. Additional screening resulted in the selection of the 3F3 anti-ferroptotic membrane antibody (3F3-FMA) as a potential ferroptosis-specific staining reagent. We validated the selectivity of 3F3-FMA by treating cells with ferroptosis inducers and inhibitors and in a comparison with two apoptosis inducers. We also tested the 3F3-FMA antibody in several cancer cell lines and identified the antigen of 3F3-FMA as transferrin receptor protein 1 (TfR1). TfR1 imports iron from the extracellular environment into cells, contributing to the cellular iron pool required for ferroptosis (Yang and Stockwell, 2008). We found that 3F3-FMA staining was localized to the plasma membrane and to a perinuclear region associated with the Golgi and the endosomal recycling compartment (ERC) by co-localization with organelle markers. We compared 3F3-FMA staining with the staining pattern of three other anti-TfR1 antibodies and anti-MDA, anti-4-HNE, and anti-ACSL4 antibodies to assess their specificity and scope of applications. We found that anti-TfR1 3B8 2A1, anti-TfR1 H68.4, anti-MDA 1F83, and anti-4-HNE ab46545 could detect ferroptotic cells in culture by immunofluorescence. Flow cytometry was sensitive enough to detect the difference between RSL3-treated and DMSO-treated cells for all tested antibodies. The 3F3-FMA and anti-TfR1 H68.4 antibodies were effective in western blotting. Anti-TfR1 3B8 2A1 and anti-MDA 1F83 antibodies provided robust results in xenograft tumor sections. In summary, these findings suggest that anti-TfR1 antibodies, including 3F3-FMA, can be used to label cells undergoing ferroptosis in cell culture and tissue samples. A combination of anti-TfR1 and anti-MDA antibodies is proposed to detect ferroptotic cells in diverse contexts. The discovery of TfR1 as a ferroptosis marker also implies that TfR1 plays a key role in ferroptosis, shedding new light on the mechanism of iron mobilization during ferroptosis.

RESULTS

Screen of 672 Monoclonal Antibodies Generated by Injecting Mice with PE-Induced Membrane Fractions

To identify a reliable and specific ferroptosis marker, we started with the generation of an untargeted pool of monoclonal antibodies by injecting mice with ferroptotic membrane fractions. Suspension OCI-LY7 cells (DLBCL, diffuse large B cell lymphoma cells) were incubated with PE, a class 1 ferroptosis inducer, for 19 h at 37°C. An increase in lipid peroxidation, confirmed by a fluorescent change in C11-BODIPY, was used as an indicator of ferroptosis to select this time point and concentration (Figure 1A). Ferroptotic cells were then lysed, homogenized, and centrifuged to obtain purified total membrane and plasma membrane fractions (see Method Details). The purified total membrane and plasma membrane were confirmed using organelle markers by western blot (Figure 1B).

Female 20-week-old mice were immunized with these membrane fractions. Following a 12-week boosting protocol, splenocytes were isolated and electrofused with a myeloma fusion partner to generate hybridoma cells (Alkan, 2004). Approximately 4,750 antibodies to unknown antigens were purified and evaluated in a high-throughput screen (Figure 1C). A total of 672 antibodies showed increased intensities in imidazole-ketone-erastin (IKE)-treated cells by flow cytometry (IKE is a system x_c^- inhibitor, similar to PE). Then, 156 of these antibodies showed increased fluorescence intensities in RSL3-treated cells by high-content analysis. We selected 71 antibodies through visual inspection to remove false positives. After cherry picking and retesting the 71 hits, 3 hits stood out, in which cells showed >3 bright spots in the cytoplasm or overall higher cytoplasmic intensity, over 5 replicates. Image analysis of 3F3-FMA is provided as an example (Figures 1D and S1).

3F3-FMA Is Identified and Validated as a Ferroptosis-Detecting Antibody

We verified the three candidate hits on a larger scale by immunofluorescence using confocal microscopy. We used RSL3 in an initial validation experiment because it is the most potent inducer, requiring low concentrations and short incubation times. Thirty percent of HT-1080 cells died after a 4-h incubation with 1 μM RSL3. 3F3-FMA was the only antibody of these three candidates showing reliable differences in staining during RSL3-induced ferroptosis. During ferroptosis, 3F3-FMA stained with greater intensity the cell boundaries, and intracellular puncta became brighter (Figure 2A). To further validate 3F3-FMA as detecting ferroptotic cells, we added the ferroptosis inhibitor ferrostatin-1 (fer-1), together with RSL3 (Figure 2A) or IKE (Figure S2A). The staining by 3F3-FMA in IKE + fer-1-treated cells was similar to DMSO-treated cells, which is consistent with 3F3-FMA being able to detect cells undergoing ferroptosis and its target antigen being suppressed by fer-1 treatment.

Quantification of membrane fluorescence intensity was subsequently used to evaluate the difference in membrane-localized antigens. We tested five additional ferroptosis inducers—IKE, erastin, ferroptosis inducer 56 (FIN56), ferroptosis inducer endoperoxide (FINO$_2$) and tBuOOH—and found that the same changes in 3F3-FMA staining were observed (Figure 2B). To test whether 3F3-FMA could differentiate ferroptosis from apoptosis, we used staurosporine (STS) to induce apoptosis and a cleaved caspase-3 antibody as a marker of

apoptosis. Accumulation of 3F3-FMA staining on the cell surface was not detected in response to STS treatment, indicating that the staining changes detected by 3F3-FMA were specific to ferroptosis over apoptosis (Figure 2C). To further test the ferroptosis specificity of 3F3-FMA, camptothecin was used to induce apoptosis in HT-1080 cells, with cleaved poly (ADP-ribose) polymerase (PARP) antibody used as an apoptosis marker. Similar to STS-treated cells, there was no significant increase in 3F3-FMA accumulation on the cell surface, further indicating that this accumulation is specific to ferroptosis.

Next, we expanded this study to other cancer cell lines. We evaluated A-673 (human muscle sarcoma) cells, SK-BR-3 (human breast cancer) cells, Huh-7 (hepatocyte-derived carcinoma) cells, and SK-LMS-1 (human leiomyosarcoma) cells, which are sensitive to ferroptosis. Again, we found that 3F3-FMA staining concentrated at the cell boundaries and became brighter upon ferroptosis induction (Figure 2D). The data indicate that the 3F3-FMA antibody can be used as a ferroptosis marker using immunofluorescence microscopy of the cells in culture.

Similar to apoptosis, nuclear shrinkage under ferroptosis was also consistently observed, with a 17% decrease in nuclear size (Figure S2B). We validated this finding by immunofluorescence (Figure S2C). The extent of shrinkage depended on the kind of inducers and incubation time. The nuclei shrank by 27% upon a 4-h incubation with 1 μM RSL3, 12% upon an 8-h incubation with 10 μM IKE, 21% upon an 8-h incubation with 15 μM erastin, 17% upon an 8-h incubation with 10 μM FIN56, and 49% upon an 8-h incubation with 15 μM FINO$_2$. This provides another reliable morphological feature of ferroptosis.

The Antigen of 3F3-FMA Is TfR1

Next, we aimed to identify the antigen of 3F3-FMA using immunoprecipitation (IP) and mass spectrometry. We incubated 3F3-FMA with an HT-1080 cell lysate overnight. Magnetic beads were added and washed, and bead-immobilized proteins were analyzed by mass spectrometry. TfR1 had the highest confidence identification as the target antigen at 63%, with 32 exclusive unique peptides, 48 exclusive unique spectra, and 53% amino acid coverage (Figure 3A). We further validated this antigen by small interfering RNA (siRNA) knockdown: siRNAs targeting TfR1 versus NT (non-targeting) siRNAs were transfected into HT-1080 cells and incubated for 48 h. After an additional 24 h, cells were fixed and stained with 3F3-FMA. In siTfR1-transfected cells, there was no detectable staining by 3F3-FMA, supporting the conclusion that the target antigen is TfR1 (Figure 3B).

Next, we aimed to better localize 3F3-FMA staining within cells. We co-localized 3F3-FMA with Tom20 (a mitochondria marker), PDI (an ER marker), and GM130 (a Golgi marker) using 2 secondary antibodies with different excitation and emission wavelengths. We found that 3F3-FMA staining was not visible in mitochondria or the ER (Figure S3). 3F3-FMA staining was instead located primarily in the region around the Golgi (Figure 3C), which is also associated with the ERC. In untreated conditions, most of the staining remained in the Golgi/ERC region (see bright dots shown by green arrows), but when ferroptosis took place, these puncta moved out of the Golgi/ERC region (Figure 3C). We further determined that these puncta moved to the plasma membrane by co-staining 3F3-FMA or TfR1 3B8 2A1

antibodies with a wheat germ agglutinin (WGA) Alexa Fluor 633 conjugate, a commonly used reagent to label glycoproteins for imaging the plasma membrane (Figure 3D). We monitored translocation by examining multiple time points upon the induction of ferroptosis by RSL3 and co-staining TfR1 with a Golgi marker. Increased accumulation of TfR1 protein in the plasma membrane and decreased localization in the Golgi/ERC region were observed during the course of RSL3 treatment (Figure 3E). This translocation was further confirmed by fixing cells without permeabilization. We found that the 3F3-FMA antibody could stain the plasma membrane in cells fixed without permeabilization, confirming membrane translocation of the TfR1 antigen (Figure 3F). The translocation of the 3F3-FMA antigen was consistent with the antigen being in the extracellular or transmembrane domains of TfR1 (Aisen, 2004).

TfR1 is the main regulator of iron uptake in cells. After binding to iron-loaded transferrin, TfR1 is enclosed within clathrin-coated endocytic vesicles and internalized by cells. Iron is then released due to endosomal acidification. Apotransferrin and its receptor are sorted in the ERC/Golgi and to some extent transported back to the cell surface. It was therefore consistent with the known trafficking of TfR1 that we observed the 3F3-FMA antigen at the plasma membrane and in the Golgi/ERC region.

Use of TfR1 Antibodies and Other Potential Ferroptosis-Staining Reagents for Immunofluorescence

In addition to 3F3-FMA, we acquired three other anti-TfR1 antibodies. Our goal was to test whether these antibodies had staining changes similar to those of 3F3-FMA, thereby further validating TfR1 as the 3F3-FMA antigen. An additional goal was to compare these anti-TfR1 antibodies to see whether one has advantages over others. To find the most specific and reliable ferroptosis marker, we also compared these TfR1 antibodies with anti-MDA, anti-4-HNE, and anti-ACSL4 antibodies, which have been explored as molecular markers of ferroptosis.

RSL3 was used to induce ferroptosis in this comparison. We found an increase in membrane intensities for anti-TfR1 3B8 2A1 and anti-TfR1 H68.4 (Figure 4A), but not for anti-TfR1 D7G9X (Figure S4A). This was not unexpected, as these antibodies have different target sequences within TfR1.

Next, we compared other potential ferroptosis-staining reagents—anti-MDA 1F83, anti-MDA ab6463, anti-4-HNE ab46545, and anti-ACSL4 sc-365230 antibodies. We found that anti-MDA 1F83 and anti-4-HNE ab46545 were capable of staining HT-1080 cells during RSL3-induced ferroptosis (Figure 4B). We saw an increase in intensities at the plasma membrane with these antibodies. However, the anti-MDA ab6463 antibody and the anti-ACSL4 sc-365230 antibody were not effective under these conditions (Figure S4A). In summary, 3F3-FMA and some other anti-TfR1 antibodies, the anti-MDA 1F83 antibody, and the anti-4-HNE ab46545 antibody can be used as ferroptosis markers using immunofluorescence in cell culture.

We then tested these antibodies for their ability to detect STS-induced apoptosis to see whether they could differentiate ferroptosis from apoptosis. An anti-cleaved-caspase-3

antibody was used to verify the induction of apoptosis (Figure 2C). Unlike in the case of ferroptosis, we found that anti-TfR1 antibody staining did not accumulate on the cell surface during apoptosis. Consistent with the formation of apoptotic bodies, TfR1 was detected outside intact cells during apoptosis (Figure 4C). Quantification did not show an increase in the intensities of anti-TfR1 antibody staining in the plasma membranes, but rather showed a slight decrease. Neither membrane-localized anti-MDA staining nor anti-4-HNE staining increased during apoptosis, indicating that both of these antibodies could differentiate ferroptosis from apoptosis (Figure 4C).

We also tested anti-TfR1 3B8 2A1, anti-TfR1 H68.4, anti-MDA 1F83, and anti-4-HNE ab46545 antibodies in camptothecin-induced apoptosis; a cleaved PARP antibody was used to detect the induction of apoptosis (Figure 2C). We found that, as with STS-induced apoptosis, TfR1 did not accumulate on the cell surface; there was rather a decrease in membrane intensity (Figure S4B). The membrane intensity of anti-MDA 1F83 and anti-4-HNE ab46545 antibodies did not change in camptothecin-treated cells. This indicates that anti-TfR1 antibodies, together with anti-MDA 1F83 and anti-4-HNE ab46545, are effective in differentiating ferroptosis from apoptosis.

Next, we sought to test whether these antibodies could differentiate between ferroptosis and more general oxidative stress that does not lead to ferroptosis. We incubated HT-1080 cells with 1 μM H_2O_2 for 4 h to test whether anti-TfR1 antibodies and other potential ferroptosis-staining reagents could differentiate ferroptosis from H_2O_2-induced cell death, which has been suggested to be a necrotic death associated with oxidative stress. We did not observe increased membrane intensities for anti-TfR1 antibodies, including 3F3-FMA, TfR1 3B8 2A1, and TfR1 H68.4 (Figure S4C). However, we did see increased cellular intensities of anti-MDA 1F83 and anti-4-HNE ab46545 antibodies in H_2O_2-treated cells (Figure S4C). Therefore, in the HT-1080 cell context, anti-TfR1 antibodies were able to differentiate ferroptosis from H_2O_2-induced oxidative stress and necrotic death, but anti-MDA and anti-4-HNE antibodies were not.

Application of TfR1 Antibodies in Flow Cytometry and Western Blotting and Comparison with Other Ferroptosis-Staining Reagents

To explore the scope of applications for these antibodies, anti-TfR1, anti-MDA, and anti-4-HNE antibodies were evaluated using flow cytometry and western blotting. We found that all of these antibodies showed increased staining intensities in RSL3-treated HT-1080 cells by flow cytometry (Figure 5A). Compared to C11-BODIPY, which is a sensor of lipid peroxidation, anti-TfR1 H68.4, anti-MDA ab6463, and anti-4-HNE ab46545 antibodies showed distinct differences between DMSO-treated and RSL3-treated cells. We also found that 3F3-FMA showed a decreased intensity in STS-induced apoptosis, indicating that 3F3-FMA can differentiate ferroptosis from apoptosis by flow cytometry (Figure 5B).

In western blotting, an increased intensity of the bands blotted by 3F3-FMA and anti-TfR1 H68.4 antibodies was detected in both RSL3-induced and IKE-induced ferroptosis, indicating an increased level or accessibility of cellular TfR1 proteins, not just a change in localization (Figure 5C). We tested whether the mRNA level of *TfR1* changed during ferroptosis using qPCR; we did not observe any difference, indicating that the amount of

TfR1 transcript was not affected during ferroptosis (Figure 5D) and that the IRP-IRE system is likely not altered during ferroptosis. We hypothesize that the increase in TfR1 protein level by western blot is due to the upregulation of translation, downregulation of proteolysis, and/or increased accessibility to the antibodies.

Applications of TfR1 Antibodies in Mouse Xenograft Tumor Tissues and Comparison with Other Potential Ferroptosis-Staining Reagents

We then tested 3F3-FMA together with other anti-TfR1 antibodies, as well as anti-MDA and anti-4-HNE antibodies in mouse xenograft tumor tissue sections. The preparation of human B cell lymphoma xenograft tissue samples was described previously (Zhang et al., 2019). Briefly, 6-week-old NCG mice were injected with 10 million SU-DHL-6 cells subcutaneously. The mice were treated after the tumor size reached 100 mm^3. Mice were randomized into treatment groups and dosed with vehicle and 40 mg/kg IKE once daily by IP for 14 days. Three hours after the final dose, mice were euthanized with CO_2 and tumor tissue was dissected, frozen, fixed, and sectioned to make slides (Figure 6A). We found that anti-TfR1 3B8 2A1, anti-TfR1 H68.4, and anti-MDA 1F83 showed significant increases in staining intensities in IKE-treated xenograft tissue samples; however, 3F3-FMA did not detect its antigen in these samples (Figure 6B)—this may require the optimization of fixation conditions for 3F3-FMA use in DLBCL xenograft tissue sections. Anti-MDA ab6463 and anti-4-HNE ab46545 showed increased intensities in IKE-treated samples as well, but to a lesser extent (Figure 6B).

Next, we generated HCC (hepatocellular carcinoma) mouse xenograft tissue samples by injecting 6-week-old NCG mice with 5 million human Huh-7 HCC cells. After 3 weeks, mice were dosed with vehicle or 50 mg/kg IKE once daily by IP for 2 days. Three hours after the final dose, mice were euthanized with CO_2 and tumor tissue was dissected, frozen, fixed, and sectioned to make slides (Figure 6A). Only 3F3-FMA, anti-TfR1 3B8 2A1, and anti-MDA 1F83 antibodies showed increased intensities in these IKE-treated HCC samples (Figure 6C). We validated that tumor cells, but not infiltrating immune cells, were stained in both of these mouse xenograft tissue samples using the cell markers CD20, CD8/45, and GPC3 (Figure S5). Overall, anti-TfR1 3B8 2A1 and anti-MDA 1F83 showed the strongest increases in both samples and are recommended as robust ferroptosis markers for frozen tissue xenograft samples.

We were also interested in determining whether 3F3-FMA could be used to detect TfR1 in normal tissues. We evaluated 3F3-FMA staining in post-mortem human brain tissues. We compared the level of staining in HD and control human brain tissues. The expression of TfR1 in brain tissue was apparently low, as evidenced by a lack of signal, and we did not detect any differences between the control group and the HD group (Figure S6A). We also evaluated 3F3-FMA in normal mouse liver frozen tissue samples. We detected a robust signal for 3F3-FMA in this tissue. This suggests that human TfR1 expression may be low in normal human brain tissue and higher in normal mouse liver, such that it may be feasible to detect ferroptosis in human brains and mouse livers in some disease contexts, if TfR1 abundance increases substantially in disease contexts.

Finally, we sought to test whether 3F3-FMA could be used in paraffin-embedded tissue samples, which are historically more abundant and accessible than fresh frozen tissues. We evaluated 3F3-FMA staining in mouse glioblastoma (GBM) paraffin-embedded tissue samples, to see whether the increased TfR1 that has been observed in many tumors would render 3F3-FMA staining detectable in this setting over the low signal evident in normal brain tissue. 3F3-FMA was indeed able to recognize mouse TfR1 protein in these tumor samples, suggesting that future studies could evaluate TfR1 levels as a ferroptosis marker in mouse, and possibly human, GBM samples (Figure S6B).

DISCUSSION

We assessed 3F3-FMA, together with three commercially available anti-TfR1 antibodies and four additional potential ferroptosis-staining reagents, in different assays (immunofluorescence, flow cytometry, and tissue sections; Table 1). Overall, the 3F3-FMA, anti-TfR1 3B8 2A1, and anti-MDA 1F83 antibodies performed well in mouse xenograft model tissue samples and in both immunofluorescence and flow cytometry applications. We propose that researchers can use a combination of these anti-TfR1 and anti-MDA 1F83 antibodies as ferroptosis markers to stain human and mouse tissue sections, which will aid in research on the role of ferroptosis in disease.

The discovery of TfR1 accumulation on the cell surface as a feature of ferroptosis is significant. Nonetheless, specificity is a potential limitation of using anti-TfR1 antibodies as ferroptosis markers. We found, however, that anti-TfR1 antibodies could differentiate ferroptosis from apoptosis; other cell death forms, including necroptosis, autophagic death, and pyroptosis, have not been tested. It was reported previously that uptake of extracellular iron by a TfR1-dependent iron transport mechanism was required in hydroperoxide-induced $2',7'$-dichlorodihydrofluorescein (DCFH) oxidation and endothelial cell apoptosis (Tampo et al., 2003). Treatment with an anti-TfR1 antibody also dramatically inhibited iron uptake, intracellular oxidant formation, and doxorubicin-induced apoptosis (Kotamraju et al., 2002). Further validation of the specificity of anti-TfR1 antibodies is therefore needed across diverse contexts before we can be certain of its suitability as a specific marker of ferroptosis.

In addition to the potential use of TfR1 as a ferroptosis marker, future studies may examine why TfR1 accumulation on the cell surface occurs during ferroptosis. One hypothesis we had was that the internalization machinery is disrupted during ferroptosis. To test this hypothesis, we examined epidermal growth factor receptor (EGFR) localization because EGFR uses the same clathrin-mediated endocytosis process as TfR1 and is internalized in the presence of EGF. We found, however, that EGFR was still internalized in the presence of EGF during ferroptosis, indicating that clathrin-mediated endocytosis is not disrupted during ferroptosis (Figure S7). Therefore, we hypothesize that recruitment of TfR1 to the plasma membrane during ferroptosis is related to altered iron metabolism, not to the disruption of trafficking. This may occur through a positive feedback cycle between iron uptake and ferroptotic death.

A further direction for the future is the study of the role of TfR1 in ferroptosis. It was reported previously that cells with knockdown of *TfR1* became more resistant to erastin-

induced cell death (Yang and Stockwell, 2008) and that siTfR1 RNAi significantly inhibited serum-dependent necrosis, which was subsequently determined to be ferroptosis (Gao et al., 2015). These results indicate that decreased iron uptake caused by the knockdown of *TfR1* is implicated in ferroptosis. However, the cellular iron pool is also controlled by an iron storage protein complex consisting of ferritin heavy chain 1 (FTH1) and ferritin light chain (FTL) (Harrison and Arosio, 1996). The precise role of TfR1 and the related iron metabolism pathway in ferroptosis remains to be determined.

TfR1 is abundantly expressed and involved in the progression of several cancers, including brain cancers, breast cancers, colon cancers, and liver cancers, suggesting that TfR1 may be a potential therapeutic target (Daniels et al., 2012). The increased need for iron uptake leads to the high expression of TfR1, because iron is required for tumor cell proliferation (Marques et al., 2016). However, the upregulation of iron uptake by TfR1 also augments the labile redox-active iron pool, which is needed for ferroptosis. Therefore, how iron metabolism is regulated between tumor progression and ferroptotic tumor suppression remains to be defined. More research is needed to define the relation between TfR1 expression, iron metabolism, ferroptosis sensitivity, and cancer progression.

In summary, we began with a pool of antibodies with unknown targets generated from membrane fractions of cells undergoing ferroptosis. The 3F3-FMA antibody was found to mark ferroptotic cells, and its antigen was identified as TfR1. Additional anti-TfR1 antibodies and other potential ferroptosis staining reagents were assessed by immunofluorescence, flow cytometry, western blotting, and tissue samples. Ultimately, 3F3-FMA, the anti-TfR1 3B8 2A1 antibody, and the anti-MDA 1F83 antibody performed well across immunofluorescence, flow cytometry, and tissue-staining applications. We recommend using these antibodies to detect cells undergoing ferroptosis in diverse contexts in the future.

STAR★METHODS

LEAD CONTACT AND MATERIALS AVAILABILITY

Further information and requests for resources and reagents should be directed to and will be fulfilled by the Lead Contact, Brent R. Stockwell (bstockwell@columbia.edu).

All unique/stable reagents generated in this study are available from the Lead Contact with a completed Materials Transfer Agreement.

EXPERIMENTAL MODEL AND SUBJECT DETAILS

Cell lines include OCI-LY7 (obtained from DSMZ), HT-1080 (obtained from ATCC), A-673 (this lab), SK-BR-3 (this lab), SK-LMS-1 (this lab) and Huh-7 (this lab). HT-1080 cells were grown in DMEM with glutamine and sodium pyruvate (Corning 10–013) supplemented with 10% heat-inactivated fetal bovine serum (FBS) (Life Technologies, 10437036) 1% non-essential amino acids (Thermo Fisher Scientific, 11140076) and 1% penicillin-streptomycin mix (pen-strep) (Thermo Fisher Scientific, 15140148). OCI-LY7 cells were grown in RPMI-1640 (ATCC 30–001) supplemented with 10% FBS and 1% Pen-Strep. A-673 cells were grown in ATCC-formulated Dulbecco's Modified Eagle's

Medium (ATCC 30–2002) supplemented with 10% FBS and 1% Pen-Strep. SK-BR-3 cells were grown in ATCC-formulated McCoy's 5a Medium Modified (ATCC 30–2007) supplemented with 10% FBS and 1% Pen-Strep. SK-LMS-1 cells were grown in ATCC-formulated Eagle's Minimum Essential Medium (ATCC 30–2003) supplemented with 10% FBS and 1% Pen-Strep. Huh-7 cells were grown in DMEM, low glucose, pyruvate (Thermo Fisher Scientific 11885084) supplemented with 10% FBS and 1% Pen-Strep. All cell lines were maintained in a humidified environment at 37°C and 5% CO_2 in an incubator.

The animal studies reported in this manuscript adhere to the ARRIVE guidelines. All animal study protocols were approved by the Columbia University Institutional Animal Care and Use Committee (IACUC). NOD-*Prkdc*[em26Cd52]Il*2rg*[em26Cd22]/NjuCrl (NCG) mice (Charles River, strain code 572) (male and female, 5-weeks of age) were acclimated after shipping for > 3 days before beginning experiments. Mice were fed a standard diet (PicoLab 5053) and maintained with no more than 5 mice per cage.

Five human HD and five unaffected control brain tissue samples are from the NIH NeuroBioBank at the Harvard Brain Tissue Resource Center, the University of Maryland, Baltimore, MD, VA_LA, the University of Pittsburgh, and the University of Miami from the caudate nucleus. The age, the sex and the developmental stage are listed as follows:

Origin	Sample Type	Sample Name	Age	Sex
Harvard	Huntington's Grade 3	AN13346	47	M
Maryland	Huntington's Grade 3	4511	78	F
Maryland	Huntington's Grade 2	5199	67	M
VA-LA	Huntington's Grade 2–3	3167	57	M
VA-LA	Huntington's Grade 3	4518	49	M
Maryland	Control	5697	67	M
PITT	Control	13108	57	M
Miami	Control	HCTYO	49	F
Miami	Control	HCT15HAO	70	M
Miami	Control	HCT15HAU	65	M

METHOD DETAILS

Generation of PE-induced membrane fractions—6 L of media (1% Pen-Strep 10% FBS and 89% RPMI with L-glutamine) containing 400 million OCI-LY7 (DSMZ Cat# ACC-688, RRID:CVCL_1881) cells/L were treated with 5 μM PE (piperazine erastin). Cells were incubated for 19 h at 37°C, then production of lipid ROS was confirmed using BODIPY-C11 by flow cytometry. Ferroptotic cells were pelleted in a ThermoFisher Scientific Sorvall Legend RT+ centrifuge at 218 × g for 10 min at 25°C. Cells were re-suspended in 1 mL lysis buffer with a pan-protease inhibitor, lysed using a dounce homogenizer. ~70% cell lysis was confirmed by microscopy. The pellet containing the nuclear fraction and unlysed cells was obtained by centrifuging at 700 × g for 10 min at 4°C. The supernatant was spun at 700 × g for 10 min at 4°C. The supernatant was then transferred to a new tube and placed in centrifuge at 10,000 × g for 45 min at 4°C. The pellet consisting

of total membrane was re-suspended in upper phase solution from Plasma Membrane Protein Extraction Kit (Abcam, Cat# ab65400). The lower phase solution from Plasma Membrane Protein Extraction Kit (Abcam, Cat# ab65400) was added and mixture was incubated on ice for 5 min. The mixture was spun at $1000 \times g$ for 5 min at 4°C. The upper phase was collected and diluted with 5x volume of H_2O and incubated on ice for 10 min. The mixture was spun at $17,000 \times g$ for 15 min at 4°C and pellet composed of plasma membrane was collected. Fractions were confirmed by western blot.

Purification of monoclonal antibodies and generation of 3F3-FMA—Murine monoclonal antibodies (including clone FH3F3) were generated at the Fred Hutchinson Antibody Technology Core Facility in Seattle Washington. Briefly, female 20-week-old mice (of various strains) were immunized with ferroptotic membrane fractions (see previous Methods). Following a 12-week boosting protocol, splenocytes were isolated from four high-titer mice and electrofused with a myeloma fusion partner to generate hybridoma cells. Approximately 4,750 hybridomas positive for IgG secretion were then identified and isolated using a ClonePix2 colony picker (Molecular Devices, CPII). Primary screening of the 4,750 clones was performed by indirect flow cytometry of ferroptotic LY-7 cells (with 5 μM IKE treatment for 19 h at 37°C, fixed with 0.01% formaldehyde in PBS for 15 min at 22°C, permeabilized in FACS buffer with 0.5% v/v Tween-20 detergent). Clones showing fluorescent staining ~4-fold over background levels (irrelevant primary antibody plus secondary antibody) were isolated for culture and frozen as the "Primary Clone Archive." Clone 3F3 was further identified within the Primary Clone Archive by fluorescent staining and high-content image analysis. Clone 3F3 was then subcloned by limiting dilution-CPII colony picking. Small-scale antibody productions in serum-free medium (GIBCO Hybridoma SFM) were carried out followed by affinity chromatography (AKTA Pure, MabSelectSuRe) to obtain ~5 mg of purified IgG1 from subclones 3F3a and 3F3h.

High-content screening and analysis

Automation: Plate and liquid handling was performed using a HTS platform system composed of a Sciclone G3 Liquid Handler from PerkinElmer (Waltham, MA, USA), a MultiFlo™ Dispenser (Biotek Instruments, Bad Friedrichshall, Germany) and a Cytomat™ Incubator (Thermo Fisher Scientific, Waltham, MA, USA) (Schorpp and Hadian, 2014). Cell seeding and assays were performed in black 384-well CellCarrier-384 Ultra Microplates (PerkinElmer, 6057300). Image acquisition and image-based quantification was performed using an Operetta®/Columbus™ high-content imaging platform (PerkinElmer, USA).

High-Content Screening assay—For screening with five technical replicates, HT-1080 cells were washed with PBS, trypsinized, and resuspended in cell culture medium. The cell suspension (2,000 cells in 50 μl per well) was dispensed into collagen (Sigma-Aldrich, St. Louis, MA, USA) pre-coated 384-well plates (PerkinElmer 384-well CellCarrierUltra™). 24 h after seeding, medium was exchanged to medium containing 0.3 μM RSL3 (1 μM stock solution) dissolved in 100% dimethyl sulfoxide (DMSO) or DMSO alone. 50 μl medium with 0.3 μM RSL3/DMSO was added per well. The cells were then incubated (37°C; 5% CO_2) for 2.5 h prior to fixation and antibody staining. After incubation, the medium was removed and cells were washed with PBS, fixed with 4% PFA for 10 min and washed again

with PBS. After permeabilizing (0.5% Tween-20) for 10 min and blocking (1% BSA in PBS) for 2 h, cells were incubated with primary antibody in blocking solution (1:20) overnight at 4°C. The following secondary antibody was applied for 1 h at room temperature: anti-mouse Alexa488 (1:500, Invitrogen). Cells were again washed with PBS and then stained with Hoechst 33342 and Phalloidin-TRITC for 1 h at room temperature in the dark and then extensively washed with PBS. Finally, plates were recorded using the automated Operetta® microscope with the $20 \times$ high NA objective for high-resolution images (PerkinElmer, USA). For quantification, three images of each condition were recorded using three channels (Hoechst, Alexa488, TRITC). This resulted in at least 100 cells for each condition in all wells. Quantification of cell number, cytoplasmic intensity, nucleus intensity, and spot number per cell was performed using Columbus Software (PerkinElmer, USA).

Image analysis—Multiparametric image analysis was performed using Columbus Software 2.8.0 (PerkinElmer). Hoechst signal was used to detect all cell nuclei. Phalloidin-TRITC was used to determine the cytoplasmic region to the corresponding nucleus. Moreover, we applied a filter to remove border objects (nuclei that cross image borders) and cells with extremely small nuclei (dead cells). In a next step, we calculated the morphology and Alexa488 fluorescence intensity in each cell region (nucleus and cytoplasm). In addition, we performed spot detection in the cytoplasm and used morphology and intensity for each spot to define "big spots." Each spot was detected as a small region within the corresponding image by having a higher intensity than its surrounding area. Furthermore, we selected cells with three or more "big spots" in the cytoplasm and calculated the percentage of "positive" cells in each well. Finally, a hit was defined if the ratio of cytoplasmic intensity and/or the ratio of cells with more than 3 spots was > 1 in at least 3 of 5 plates after RSL3 treatment. An illustration on the automated detection method using the Hoechst, phalloidin-TRITC- and Alexa488 antibody- signal is presented in Figure S1.

Immunofluorescence (IF)—HT-1080 (ATCC Cat# CRL-7951, RRID:CVCL_0317), A-673, SK-BR-3, SK-LMS-1 and Huh-7 cells were treated with 1 μM RSL3 for 4 h, 15 μM erastin for 8 h, 10 μM IKE for 8 h, 15 μM FINO$_2$ for 8 h, 10 μM FIN56 for 8 h, 100 μM tBuOOH for 8 h, 1 μM staurosporine (STS) for 6 h, 2 μM camptothecin (CPT) for 24 h, 1 μM RSL3 + 5 μM Fer-1 for 4 h and 10 μM IKE + 5 μM Fer-1 for 8 h on poly-lysine-coated coverslips (Sigma Aldrich P4832) in 24-well plate. Medium was removed and the cells were gently washed with PBS^{2+} (PBS with 1 μM CaCl$_2$ and 0.5 μM MgCl$_2$) twice. The cells were fixed and permeabilized by adding 200 μL/well of 4% paraformaldehyde (PFA) in PBS with 0.1% Triton X-100 (PBT), and incubated at room temperature for 18 min. The cells were then washed with PBT three times. Then the cells were blocked with 5% goat serum (ThermoFisher 50197Z) in PBT for 1 h at room temperature. The cells were incubated with purified mouse monoclonal antibodies (1:5 dilution), mouse mAb 3F3-FMA (1:500 dilution), Transferrin Receptor/CD71 Monoclonal Antibody, Clone: H68.4, Invitrogen (Thermo Fisher Scientific Cat# 13–6800, RRID:AB_2533029, 1:250 dilution), Cd71 (D7G9X) XP® Rabbit mAb (Cell Signaling Technology Cat# 13113, RRID:AB_2715594, 1:100 dilution), CD71 (3B8 2A1) (Santa Cruz Biotechnology Cat# sc-32272, RRID:AB_627167, 1:50 dilution), Tom20 (FL-145) (Santa Cruz Biotechnology Cat#

sc-11415, RRID:AB_2207533, 1:250 dilution), anti-PDI antibody [RL90] - ER Marker (Abcam Cat# ab2792, RRID:AB_303304, 1:100 dilution), anti-Gm130 (D6B1) XP® Rabbit mAb (Cell Signaling Technology Cat# 12480, RRID:AB_2797933, 1:3200 dilution), anti-malondialdehyde antibody (Abcam Cat# ab6463, RRID:AB_305484, 1:400 dilution), anti-4-hydroxynonenal antibody (Abcam Cat# ab46544, RRID:AB_722493, 1:50 dilution), anti-ACSL4 antibody (F-4) (Santa Cruz Biotechnology Cat# sc-365230, RRID:AB_10843105, 1:50 dilution), mouse mAb 1F83 (1:100 dilution), which recognizes the malondialdehyde-(MDA)-lysine adduct 4-methyl-1,4-dihydropyridine-3,5-dicarbaldehyde (MDHDC) (Yamada et al., 2001), in PBT with 1% BSA and 5% goat serum overnight at 4°C. The cells were washed with PBT for 5 min three times. The cells were incubated with goat anti-mouse IgG (H+L) Highly Cross-Adsorbed Secondary Antibody, Alexa Fluor 594 (Thermo Fisher Scientific Cat# A-11032, RRID:AB_2534091, 1:200 dilution) or goat anti-rabbit IgG (H+L) Highly Cross-Adsorbed Secondary Antibody, Alexa Fluor 488 (Thermo Fisher Scientific Cat# A-11034, RRID:AB_2576217, 1:200 dilution) at room temperature for 1 h. The cells were washed with PBT for 5 min three times. ProLong Diamond anti-fade mountant with DAPI (ThermoFisher P36962) was added to stain the nucleus. All images were captured on a Zeiss LSM 800 confocal microscope at Plan-Apochromat 63x/1.40 oil DIC objective with constant laser intensity for all samples. When applicable, line-scan analysis was performed on representative confocal microscopy images using Zeiss LSM software to qualitatively visualize fluorescence overlap.

Quantification method—The quantification of the intensity of antibodies was analyzed using CellProfiler 3.1.8 (Carpenter et al., 2006) (CellProfiler Image Analysis Software, RRID:SCR_007358). Nuclei were first identified as primary objects using global minimum cross entropy strategy. Cytoplasms were then identified as secondary objects based on primary objects by propagation using global minimum cross entropy strategy. The plasma membranes were identified as the outermost 5 pixels of cytoplasm. Then mean intensities and size areas of nuclei, cytoplasm and plasma membranes were measured and reported. Graphs were created in Prism 7.

Immunoprecipitation-mass spectrometry (IP-MS)—HT-1080 cells were seeded in DMEM (Corning 10–013-CM) and 10% Hi-FBS with 1% penicillin and streptomycin (PS) with 1% MEM Non-Essential Amino Acids Solution (100X) (Thermo Fisher Scientific 11140–076) 16 h prior to use. DMSO or 1 μM of RSL3 was added and incubated for 4 h. Following treatment, the medium was aspirated from each dish and cells were washed twice with PBS. Cells were lysed with 70 μl lysis buffer (RIPA buffer from ThermoFisher, cat. 89900, 1 mM EDTA, 1 mM PMSF, 1X Halt™ protease inhibitor cocktail from ThermoFisher, cat. 78430 and 1X Halt™ phosphatase inhibitor cocktail from ThermoFisher, cat. 78426). Unlysed cells and debris were pelleted for 15 min at $16,000 \times g$ at 4°C. The samples were incubated with 10 μg of 3F3-FMA overnight at 4°C with shaking. The next day, Thermo Scientific Pierce Protein AG Magnetic Beads (Thermo Fisher Scientific 88802) were washed with TBS with 0.05% Tween 20 (wash buffer) and then were incubated with sample/antibody mixture for 1 h with mixing. The beads were collected with a magnetic stand and then washed with wash buffer for three times. The beads were used for mass spectrometry.

Trypsin digestion was performed overnight at 37°C. Supernatants were collected and dried down in a speed-vac, and peptides were dissolved in a solution containing 3% acetonitrile and 0.1% formic acid. Peptides were desalted with C18 disk-packed stage-tips. Desalted peptides were injected onto an EASY-Spray PepMap RSLC C18 50 cm × 75 μm column (Thermo Scientific), which was coupled to the Orbitrap Fusion Tribrid mass spectrometer (Thermo Scientific). Peptides were eluted with a non-linear 110 min gradient of 5%–30% buffer B (0.1% (v/v) formic acid, 100% acetonitrile) at a flow rate of 250 nl/min. The column temperature was maintained at a constant 50°C during all experiments. Thermo Scientific Orbitrap Fusion Tribrid mass spectrometer was used for peptide MS/MS analysis. Survey scans of peptide precursors were performed from 400 to 1575 *m/z* at 120K FWHM resolution (at 200 *m/z*) with a 2×10^5 ion count target and a maximum injection time of 50 ms. The instrument was set to run in top speed mode with 3 s cycles for the survey and the MS/MS scans. After a survey scan, tandem MS was performed on the most abundant precursors exhibiting a charge state from 2 to 6 of greater than 5×10^3 intensity by isolating them in the quadrupole at 1.6 Th. CID fragmentation was applied with 35% collision energy and resulting fragments were detected using the rapid scan rate in the ion trap. The AGC target for MS/MS was set to 1×10^4 and the maximum injection time limited to 35 ms. The dynamic exclusion was set to 45 s with a 10 ppm mass tolerance around the precursor and its isotopes. Monoisotopic precursor selection was enabled.

MS data analysis—Raw mass spectrometric data were analyzed using MaxQuant v.1.6.1.0 (Cox and Mann, 2008) (MaxQuant, RRID:SCR_014485) and employed Andromeda for database search (Cox et al., 2011) at default settings with a few modifications. The default was used for first search tolerance and main search tolerance: 20 ppm and 6 ppm, respectively. MaxQuant was set up to search the reference Human proteome database downloaded from Uniprot. MaxQuant performed the search trypsin digestion with up to 2 missed cleavages. Peptide, Site and Protein FDR were all set to 1% with a minimum of 1 peptide needed for Identification but 2 peptides needed to calculate a protein level ratio. The following modifications were used as fixed carbamidomethyl modification of cysteine, and oxidation of methionine (M), Deamination for asparagine or glutamine (NQ) and acetylation on N-terminal of protein were used as variable modifications. MaxQuant combined folder was uploaded in scaffold for data visualization.

siRNA knockdown assay—10 μM siRNAs was combined with 250 μL of Opti-MEM serum-free media (Life Technologies 31985–070) in one tube. 6 μL of Lipofectamine RNAiMAX (Thermo Fisher Scientific 13778150) was combined with 250 μL of Opti-Mem media in another tube. They were equilibrated at r.t. for 5 min. Then two tubes were combined, transferred into 6-well plate and incubated at 37°C for 20 min. 0.25 million HT-1080 cells were then added to 6-well plate and incubated for 48 h. Cells were reseeded in regular media for additional 24 h. Then regular IF procedure was conducted.

Flow cytometry and analysis—Cells were re-suspended in 500 mL HBSS containing 2 μM C11-BODIPY (BODIPY 581/591 C11) (Thermo Fisher Scientific, D3861) and incubated at 37°C for 15 min. Cells were pelleted and resuspended in HBSS strained through a 35 μm cell strainer (Fisher Scientific 08-771-23). Fluorescence intensity was

measured on the FL1 channel with gating to record live cells only (gate constructed from DMSO treatment group). A minimum of 10,000 cells were analyzed per condition. Analysis was performed using FlowJo software.

HT-1080 cells were treated with DMSO or 1 μM RSL3 for 4 h. The cells were harvested by 0.25% Trypsin-EDTA (1X) (Invitrogen 25200–114) and washed with HBSS once. The cells were re-suspended in 5% goat serum (ThermoFisher 50197Z) for 30 min on ice. The cells were incubated with mAb 3F3-FMA (1:500 dilution), Transferrin Receptor/CD71 Monoclonal Antibody, Clone: H68.4, Invitrogen (Thermo Fisher Scientific Cat# 13–6800, RRID:AB_2533029, 1:250 dilution), CD71 (3B8 2A1) (Santa Cruz Biotechnology Cat# sc-32272, RRID:AB_627167, 1:50 dilution), anti-malondialdehyde antibody (Abcam Cat# ab6463, RRID:AB_305484, 1:400 dilution), anti-4-hydroxynonenal antibody (Abcam Cat# ab46544, RRID:AB_722493, 1:50 dilution), and mouse mAb 1F83 (1:100 dilution), which specifically recognizes the malondialdehyde-(MDA)-lysine adduct 4-methyl-1,4-dihydropyridine-3,5-dicarbaldehyde (MDHDC) (Yamada et al., 2001) for 1 h on ice. The cells were washed with HBSS for 5 min three times by centrifugation. The cells were incubated with goat anti-mouse IgG (H+L) secondary antibody, Alexa Fluor® 488 conjugate (Thermo Fisher Scientific Cat# A-11001, RRID:AB_2534069, 1:200 dilution) or goat anti-rabbit IgG (H+L) Highly Cross-Adsorbed Secondary Antibody, Alexa Fluor 488 (Thermo Fisher Scientific Cat# A-11034, RRID:AB_2576217, 1:200 dilution) for 30 min on ice. The cells were washed with HBSS twice by centrifugation, then re-suspended in HBSS strained through a 35 μm cell strainer (Fisher Scientific 08-771-23). Fluorescence intensity was measured on the FL1 channel with gating to record live cells only (gate constructed from DMSO treatment group). A minimum of 10,000 cells were analyzed per condition. Analysis was performed using FlowJo software (FlowJo, RRID:SCR_008520).

Western blot—HT-1080 cells were seeded in DMEM (Corning 10–013-CM) and 10% Hi-FBS with 1% penicillin and streptomycin (PS) with 1% MEM Non-Essential Amino Acids Solution (100X) (Thermo Fisher Scientific 11140–076) 16 h prior to use. DMSO, 1 μM RSL3 or 10 μM IKE were added and incubated for 2 h and 4 h respectively. Following treatment, the medium was aspirated from each dish and cells were washed twice with PBS. Cells were lysed with 70 μl lysis buffer (RIPA buffer from ThermoFisher, cat. 89900, 1 μM EDTA, 1 μM PMSF, 1X Halt™ protease inhibitor cocktail from ThermoFisher, cat. 78430 and 1X Halt™ phosphatase inhibitor cocktail from ThermoFisher, cat. 78426). Unlysed cells and debris were pelleted for 15 min at $16,000 \times g$ at 4°C. Samples were separated using SDS-PAGE and transferred to a polyvinylidene difluoride membrane. Transfer was performed using the iBlot2 system (Invitrogen). Membranes were treated with Li-COR Odyssey blocking buffer for at least 1 h at r.t., then incubated with mouse mAb 3F3-FMA (1:500 dilution), Transferrin Receptor/CD71 Monoclonal Antibody, Clone: H68.4, Invitrogen (Thermo Fisher Scientific Cat# 13–6800, RRID:AB_2533029, 1:250 dilution), Cd71 (D7G9X) XP® Rabbit mAb (Cell Signaling Technology Cat# 13113, RRID:AB_2715594, 1:100 dilution), CD71 (3B8 2A1) (Santa Cruz Biotechnology Cat# sc-32272, RRID:AB_627167, 1:50 dilution) in a 1:1 solution of PBS-T (PBS with 0.1% Tween 20) and Li-COR odyssey blocking buffer overnight at 4°C. Following three 5 min washes in PBS-T, the membrane was incubated with secondary antibodies, goat anti-rabbit

or goat anti-mouse IgG antibody conjugated to an IRdye at 800CW (LI-COR Biosciences Cat# 926–32211, RRID:AB_621843, 1:3000 dilution) and Alexa Fluor 680 goat anti-mouse IgG (H+L) (Thermo Fisher Scientific Cat# A-21058, RRID:AB_2535724, 1:3000 dilution) in a 1:1 solution of PBS-T and Li-COR Odyssey blocking buffer for 1 h at r.t. Following three 5 min washes in PBS-T, the membrane was scanned using the Li-COR Odyssey Imaging System.

qPCR—HT-1080 cells were seeded in 6-well plates at a density of 400k cells/well and incubated overnight. The following day, IKE or RSL3 were diluted into wells from stock solutions and treated for indicated time periods. Following treatment, cells were rinsed in cold PBS, trypsinized, and pelleted in Eppendorf tubes. RNA was isolated from cell pellets using QIAGEN's RNeasy extraction kit, following manufacturer's instructions (QIAGEN). RNA quantity and quality was evaluated by a nanodrop spectrophotometer (Thermo Fisher Scientific). cDNA was generated from 2 μg of total RNA, which was then diluted ten-fold and used as a template in qPCR reactions on a Viia7 Real-Time system. Gene specific primers were used as follows: TfR1 FWD: 5′ ACCATTGTCATATACCCGGTTCA 3′; TFR1 RV: 5′ CAATAGCCCAAGTAGCCAATCAT 3′; GAPDH FW: 5′ CTCCAAAATCAAGTGGGGCG 3′; GAPDH RV: 5′ ATGACGAA CATGGGGGCATC 3′.

Animal models

B cell lymphoma mouse xenograft model: B cell lymphoma mouse xenograft model was generated by injecting 6-week-old NCG mice with 10 million SU-DHL-6 cells subcutaneously. The mice were treated after the tumor size reached 100 mm^3. Mice were separated randomly into treatment groups of 3 and dosed with vehicle and 40 mg/kg IKE once daily by IP for 14 days. 3 h after the final dosage, mice were euthanized with CO_2, and tumors were dissected, frozen on dry ice, and stored at −80°C. All experiments using animals were performed according to protocols approved by the Institutional Animal Care and Use Committee (IACUC) at Columbia University, NY, USA.

Hepatocellular carcinoma (HCC) mouse xenograft model—Hepatocellular carcinoma (HCC) mouse xenograft tissue samples were generated by injecting 6-week-old NCG mice (2 male and 2 female per group) with 5 million human Huh-7 HCC cells subcutaneously. After three weeks, mice were dosed with vehicle or 50 mg/kg IKE once daily by IP for 2 days. 3 h after the final dosage, mice were euthanized with CO_2. Tumors and liver tissues were dissected, frozen on dry ice, and stored at −80°C. All experiments using animals were performed according to protocols approved by the Institutional Animal Care and Use Committee (IACUC) at Columbia University, NY, USA.

Murine glioma model—All procedures were performed according to the Columbia University Medical Center Institutional Animal Care and Use Committee. Murine glioma cell lines were created from tumor bearing mice. These tumors were generated by injection of a PDGF-IRES-Cre retrovirus into the subcortical white matter of mice with floxed PTEN and/or p53 (Sonabend et al., 2013). After mice reached end stage, the tumors were dissociated and primary cell cultures were created. These cells harbored the specific mutations of the original tumors, and could be re-injected to form gliomas in c57/B6 mice

with high fidelity. Briefly, mice between the age of 6–8 weeks received 50,000 murine glioma cells through stereotactic injection after being anesthetized with a ketamine/xylazine cocktail (87.5mg/12.5mg w/w). After cessation of toe-pinch reflex, the scalp was shaved and cleaned with serial use of betadine and 70% ethanol swabs. An incision was made and the skull was exposed. A burr hole was created, 2 mm anterior, 2 mm lateral and 2 mm deep to the right of the bregma. The cells were injected into the subcortical white matter over a period of 3 minutes (0.333 uL/min). Once the injection ceased, the needle was left in place for 1 minute before being slowly withdrawn. After tumor developed, brains were harvested and fixed in 4% paraformaldehyde and embedded in paraffin. 5 micron sections were made for staining.

Immunohistochemistry (IHC)—Lymphoma mouse xenograft tumor tissues were prepared by Dr. Yan Zhang, HCC mouse xenograft tumor tissues were prepared by Dr. Presha Rajbhandari. Tumor tissues were fixed in 4% paraformaldehyde (PFA) for 24 h at 4°C followed by washing with PBS three times. The tissues were perfused in 30% sucrose for 24 h at 4°C for cryo-protection. The samples were embedded in OCT cryostat sectioning medium, and then moved directly into a cryostat. After equilibration of temperature, frozen tumor tissues were cut into 5 μm thick sections. Tissue sections were mounted on to poly-L-lysine coated slides by placing the cold sections onto warm slides. Slides were stored at −80°C until staining. For staining, slides were warmed to room temperature followed by washing with PBS twice. A hydrophobic barrier pen was used to draw a circle on each slide. The slides were permeabilized with PBS with 0.4% Triton X-100 (PBT) twice before non-specific-binding blocking by incubating the sections with 10% goat serum (ThermoFisher 50197Z) for 30 min at room temperature. The sections were separately incubated with mouse mAb 3F3-FMA (1:500 dilution), Transferrin Receptor/CD71 Monoclonal Antibody, Clone: H68.4, Invitrogen (Thermo Fisher Scientific Cat# 13–6800, RRID:AB_2533029, 1:250 dilution), CD71 (3B8 2A1) (Santa Cruz Biotechnology Cat# sc-32272, RRID:AB_627167, 1:50 dilution), anti-malondialdehyde antibody (Abcam Cat# ab6463, RRID:AB_305484, 1:400 dilution), anti-4-hydroxynonenal antibody (Abcam Cat# ab46544, RRID:AB_722493, 1:50 dilution), mouse mAb 1F83 (1:100 dilution), which specifically recognizes the malondialdehyde-(MDA)-lysine adduct 4-methyl-1,4-dihydropyridine-3,5-dicarbaldehyde (MDHDC) (Yamada et al., 2001), CD20 (Abcam Cat# ab194970, 1:400 dilution), GPC3 (Thermo Fisher Scientific Cat# PA5–47256, RRID: AB_2608607, 1:500 dilution), CD8 (Cell Signaling Technology Cat# 85336S, 1:300 dilution), and CD45 (Cell Signaling Technology Cat# 13917S, 1:500 dilution) overnight at 4°C in humidified chambers. Sections were washed with PBT for three times before incubating with goat anti-mouse IgG (H+L) Highly Cross-Adsorbed Secondary Antibody, Alexa Fluor 594 (Thermo Fisher Scientific Cat# A-11032, RRID:AB_2534091, 1:1000 dilution) or goat anti-Rrabbit IgG (H+L) Highly Cross-Adsorbed Secondary Antibody, Alexa Fluor 488 (Thermo Fisher Scientific Cat# A-11034, RRID:AB_2576217, 1:1000 dilution) at room temperature for 1 h. Slides were then washed twice with PBT three times. ProLong Diamond antifade mountant with DAPI (ThermoFisher P36962) was added onto slides, which were then covered with the coverslips, sealed by clear fingernail polish and observed under confocal microscopy. All images were captured on a Zeiss LSM 800 confocal microscope at Plan-Apochromat 63x/1.40 Oil DIC objective with constant laser intensity for all analyzed samples. The intensity

above threshold of the fluorescent signal of the bound antibodies was analyzed using NIH ImageJ software (ImageJ, RRID:SCR_003070). Data were expressed as fold change comparing with the vehicle.

QUANTIFICATION AND STATISTICAL ANALYSIS

Statistical analyses include one-way ANOVA and two-tailed t test. Software used include Columbus Software 2.8.0, CellProfiler 3.1.8, Prism, Version 7.0 and MaxQuant v.1.6.1.0. Statistical details of experiments can be found in the figures and figure legends, including the statistical tests used, exact value of n, what n represents, definition of center, and dispersion and precision measures.

DATA AND CODE AVAILABILITY

The mass spectrometry proteomic data have been deposited to the ProteomeXchange Consortium (http://proteomecentral.proteomexchange.org) via the PRIDE (Vizcaíno et al., 2013) partner repository with the dataset identifier PXD017425.

Supplementary Material

Refer to Web version on PubMed Central for supplementary material.

ACKNOWLEDGMENTS

REFERENCES

Aisen P (2004). Transferrin receptor 1. Int. J. Biochem. Cell Biol 36, 2137–2143. [PubMed: 15313461]

Alkan SS (2004). Monoclonal antibodies: the story of a discovery that revolutionized science and medicine. Nat. Rev. Immunol 4, 153–156. [PubMed: 15040588]

Carpenter AE, Jones TR, Lamprecht MR, Clarke C, Kang IH, Friman O, Guertin DA, Chang JH, Lindquist RA, Moffat J, et al. (2006). CellProfiler: image analysis software for identifying and quantifying cell phenotypes. Genome Biol. 7, R100. [PubMed: 17076895]

Cox J, and Mann M (2008). MaxQuant enables high peptide identification rates, individualized p.p.b.-range mass accuracies and proteome-wide protein quantification. Nat. Biotechnol 26, 1367–1372. [PubMed: 19029910]

Cox J, Neuhauser N, Michalski A, Scheltema RA, Olsen JV, and Mann M (2011). Andromeda: a peptide search engine integrated into the MaxQuant environment. J. Proteome Res 10, 1794–1805. [PubMed: 21254760]

Daniels TR, Bernabeu E, Rodríguez JA, Patel S, Kozman M, Chiappetta DA, Holler E, Ljubimova JY, Helguera G, and Penichet ML (2012). The transferrin receptor and the targeted delivery of therapeutic agents against cancer. Biochim. Biophys. Acta 1820, 291–317. [PubMed: 21851850]

Dixon SJ, and Stockwell BR (2019). The Hallmarks of Ferroptosis. Annu. Rev. Cancer Biol 3, 35–54.

Dixon SJ, Patel DN, Welsch M, Skouta R, Lee ED, Hayano M, Thomas AG, Gleason CE, Tatonetti NP, Slusher BS, and Stockwell BR (2014). Pharmacological inhibition of cystine-glutamate exchange induces endoplasmic reticulum stress and ferroptosis. eLife 3, e02523. [PubMed: 24844246]

Dixon SJ, Winter GE, Musavi LS, Lee ED, Snijder B, Rebsamen M, Superti-Furga G, and Stockwell BR (2015). Human Haploid Cell Genetics Reveals Roles for Lipid Metabolism Genes in Nonapoptotic Cell Death. ACS Chem. Biol 10, 1604–1609. [PubMed: 25965523]

Doll S, Proneth B, Tyurina YY, Panzilius E, Kobayashi S, Ingold I, Irmler M, Beckers J, Aichler M, Walch A, et al. (2017). ACSL4 dictates ferroptosis sensitivity by shaping cellular lipid composition. Nat. Chem. Biol 13, 91–98. [PubMed: 27842070]

Dolma S, Lessnick SL, Hahn WC, and Stockwell BR (2003). Identification of genotype-selective antitumor agents using synthetic lethal chemical screening in engineered human tumor cells. Cancer Cell 3, 285–296. [PubMed: 12676586]

Drummen GP, van Liebergen LC, Op den Kamp JA, and Post JA (2002). C11-BODIPY(581/591), an oxidation-sensitive fluorescent lipid peroxidation probe: (micro)spectroscopic characterization and validation of methodology. Free Radic. Biol. Med 33, 473–490. [PubMed: 12160930]

Feng H, and Stockwell BR (2018). Unsolved mysteries: how does lipid peroxidation cause ferroptosis? PLoS Biol. 16, e2006203. [PubMed: 29795546]

Gao M, Monian P, Quadri N, Ramasamy R, and Jiang X (2015). Glutaminolysis and Transferrin Regulate Ferroptosis. Mol. Cell 59, 298–308. [PubMed: 26166707]

Gaschler MM, Andia AA, Liu H, Csuka JM, Hurlocker B, Vaiana CA, Heindel DW, Zuckerman DS, Bos PH, Reznik E, et al. (2018). FINO$_2$ initiates ferroptosis through GPX4 inactivation and iron oxidation. Nat. Chem. Biol 14, 507–515. [PubMed: 29610484]

Hangauer MJ, Viswanathan VS, Ryan MJ, Bole D, Eaton JK, Matov A, Galeas J, Dhruv HD, Berens ME, Schreiber SL, et al. (2017). Drug-tolerant persister cancer cells are vulnerable to GPX4 inhibition. Nature 551, 247–250. [PubMed: 29088702]

Harrison PM, and Arosio P (1996). The ferritins: molecular properties, iron storage function and cellular regulation. Biochim. Biophys. Acta 1275, 161–203. [PubMed: 8695634]

Kotamraju S, Chitambar CR, Kalivendi SV, Joseph J, and Kalyanaraman B (2002). Transferrin receptor-dependent iron uptake is responsible for doxorubicin-mediated apoptosis in endothelial cells: role of oxidant-induced iron signaling in apoptosis. J. Biol. Chem 277, 17179–17187. [PubMed: 11856741]

Larraufie MH, Yang WS, Jiang E, Thomas AG, Slusher BS, and Stockwell BR (2015). Incorporation of metabolically stable ketones into a small molecule probe to increase potency and water solubility. Bioorg. Med. Chem. Lett 25, 4787–4792. [PubMed: 26231156]

Marques O, Porto G, Rêma A, Faria F, Cruz Paula A, Gomez-Lazaro M, Silva P, Martins da Silva B, and Lopes C (2016). Local iron homeostasis in the breast ductal carcinoma microenvironment. BMC Cancer 16, 187. [PubMed: 26944411]

Müller T, Dewitz C, Schmitz J, Schröder AS, Bräsen JH, Stockwell BR, Murphy JM, Kunzendorf U, and Krautwald S (2017). Necroptosis and ferroptosis are alternative cell death pathways that operate in acute kidney failure. Cell. Mol. Life Sci 74, 3631–3645. [PubMed: 28551825]

Schorpp K, and Hadian K (2014). Small molecule screening at Helmholtz Zentrum München - from biology to molecules. Comb. Chem. High Throughput Screen 17, 266–271. [PubMed: 24409952]

Shimada K, Skouta R, Kaplan A, Yang WS, Hayano M, Dixon SJ, Brown LM, Valenzuela CA, Wolpaw AJ, and Stockwell BR (2016). Global survey of cell death mechanisms reveals metabolic regulation of ferroptosis. Nat. Chem. Biol 12, 497–503. [PubMed: 27159577]

Skouta R, Dixon SJ, Wang J, Dunn DE, Orman M, Shimada K, Rosenberg PA, Lo DC, Weinberg JM, Linkermann A, and Stockwell BR (2014). Ferrostatins inhibit oxidative lipid damage and cell death in diverse disease models. J. Am. Chem. Soc 136, 4551–4556. [PubMed: 24592866]

Sonabend AM, Yun J, Lei L, Leung R, Soderquist C, Crisman C, Gill BJ, Carminucci A, Sisti J, Castelli M, et al. (2013). Murine cell line model of proneural glioma for evaluation of anti-tumor therapies. J. Neurooncol 112, 375–382. [PubMed: 23504257]

Stockwell BR, Friedmann Angeli JP, Bayir H, Bush AI, Conrad M, Dixon SJ, Fulda S, Gascón S, Hatzios SK, Kagan VE, et al. (2017). Ferroptosis: A Regulated Cell Death Nexus Linking Metabolism, Redox Biology, and Disease. Cell 171, 273–285. [PubMed: 28985560]

Tampo Y, Kotamraju S, Chitambar CR, Kalivendi SV, Keszler A, Joseph J, and Kalyanaraman B (2003). Oxidative stress-induced iron signaling is responsible for peroxide-dependent oxidation of dichlorodihydrofluorescein in endothelial cells: role of transferrin receptor-dependent iron uptake in apoptosis. Circ. Res 92, 56–63. [PubMed: 12522121]

Viswanathan VS, Ryan MJ, Dhruv HD, Gill S, Eichhoff OM, Seashore-Ludlow B, Kaffenberger SD, Eaton JK, Shimada K, Aguirre AJ, et al. (2017). Dependency of a therapy-resistant state of cancer cells on a lipid peroxidase pathway. Nature 547, 453–457. [PubMed: 28678785]

Vizcaíno JA, Côté RG, Csordas A, Dianes JA, Fabregat A, Foster JM, Griss J, Alpi E, Birim M, Contell J, et al. (2013). The PRoteomics IDEntifications (PRIDE) database and associated tools: status in 2013. Nucleic Acids Res. 41 (D1), D1063–D1069. [PubMed: 23203882]

Weiland A, Wang Y, Wu W, Lan X, Han X, Li Q, and Wang J (2019). Ferroptosis and Its Role in Diverse Brain Diseases. Mol. Neurobiol 56, 4880–4893. [PubMed: 30406908]

Yamada S, Kumazawa S, Ishii T, Nakayama T, Itakura K, Shibata N, Kobayashi M, Sakai K, Osawa T, and Uchida K (2001). Immunochemical detection of a lipofuscin-like fluorophore derived from malondialdehyde and lysine. J. Lipid Res 42, 1187–1196. [PubMed: 11483619]

Yamanaka K, Saito Y, Sakiyama J, Ohuchi Y, Oseto F, and Noguchi N (2012). A novel fluorescent probe with high sensitivity and selective detection of lipid hydroperoxides in cells. RSC Adv. 2, 7894–7900.

Yang WS, and Stockwell BR (2008). Synthetic lethal screening identifies compounds activating iron-dependent, nonapoptotic cell death in oncogenic-RAS-harboring cancer cells. Chem. Biol 15, 234–245. [PubMed: 18355723]

Yang WS, SriRamaratnam R, Welsch ME, Shimada K, Skouta R, Viswanathan VS, Cheah JH, Clemons PA, Shamji AF, Clish CB, et al. (2014). Regulation of ferroptotic cancer cell death by GPX4. Cell 156, 317–331. [PubMed: 24439385]

Yuan H, Li X, Zhang X, Kang R, and Tang D (2016). Identification of ACSL4 as a biomarker and contributor of ferroptosis. Biochem. Biophys. Res. Commun 478, 1338–1343. [PubMed: 27565726]

Zhang Y, Tan H, Daniels JD, Zandkarimi F, Liu H, Brown LM, Uchida K, O'Connor OA, and Stockwell BR (2019). Imidazole Ketone Erastin Induces Ferroptosis and Slows Tumor Growth in a Mouse Lymphoma Model. Cell Chem. Biol 26, 623–633.e9. [PubMed: 30799221]

Highlights

- 3F3-FMA is identified in a screen as a selective ferroptosis-immunostaining reagent

- The antigen of 3F3-FMA is identified as the transferrin receptor 1 protein (TfR1)

- Anti-TfR1 antibodies can detect ferroptosis by immunofluorescence and flow cytometry

- Anti-TfR1 and anti-MDA antibodies detect ferroptosis in xenograft cancer models
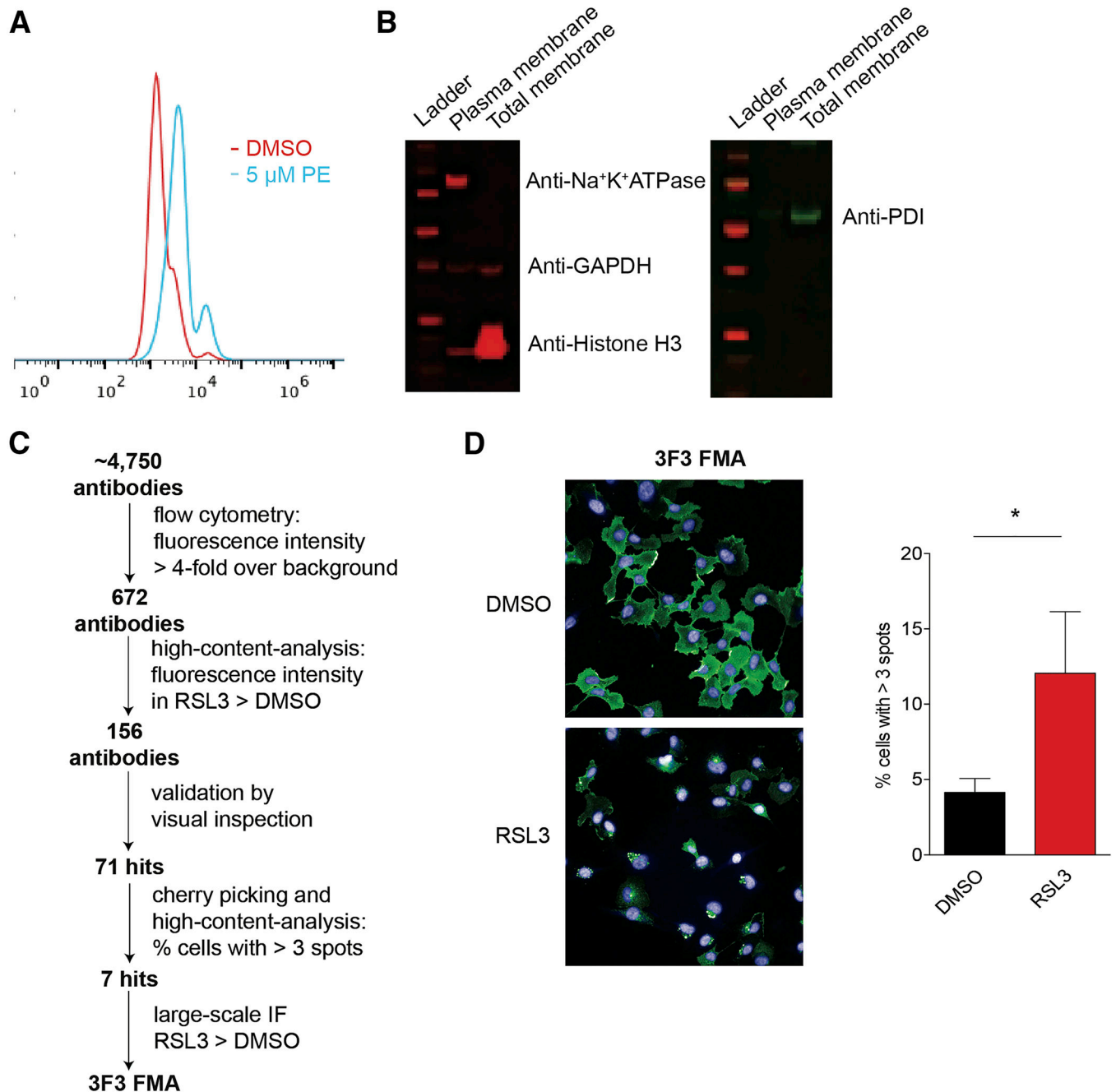
A

- DMSO
- 5 μM PE

10^0 10^2 10^4 10^6

B

Anti-Na⁺K⁺ATPase

Anti-GAPDH

Anti-Histone H3

Anti-PDI

C

~4,750
antibodies

flow cytometry:
fluorescence intensity
> 4-fold over background

672
antibodies

high-content-analysis:
fluorescence intensity
in RSL3 > DMSO

156
antibodies

validation by
visual inspection

71 hits

cherry picking and
high-content-analysis:
% cells with > 3 spots

7 hits

large-scale IF
RSL3 > DMSO

3F3 FMA

D

3F3 FMA

DMSO

RSL3

$*$

% cells with > 3 spots

DMSO   RSL3

Figure 1. Screen of 672 Monoclonal Antibodies Generated by Infecting Mice with PE-Induced Membrane Fractions

(A) Cells were confirmed to be undergoing ferroptosis by using the fluorescent probe C11-BODIPY as a lipid ROS indicator. Blue represents DMSO-treated cells. Red represents PE-treated cells.

(B) Western blot confirmation of plasma membrane and total membrane by organelle markers. The presence of plasma membrane was determined by anti-sodium potassium ATPase antibody, cytosol by anti-glyceraldehyde 3-phosphate dehydrogenase (GAPDH), ER by anti-PDI, and nuclei by anti-histone H3.

(C) A flowchart illustrating the screen from ~4,750 unknown target antibodies to 3F3-FMA by flow cytometry, immunofluorescence, and high-content image analysis.

(D) 3F3-FMA is shown as an example of cherry picking and high-content-analysis. There was an increased number of cells, which had >3 spots in cytoplasm in RSL3-induced ferroptosis. *p $\leq$ 0.05. Data plotted are mean ± SEM.
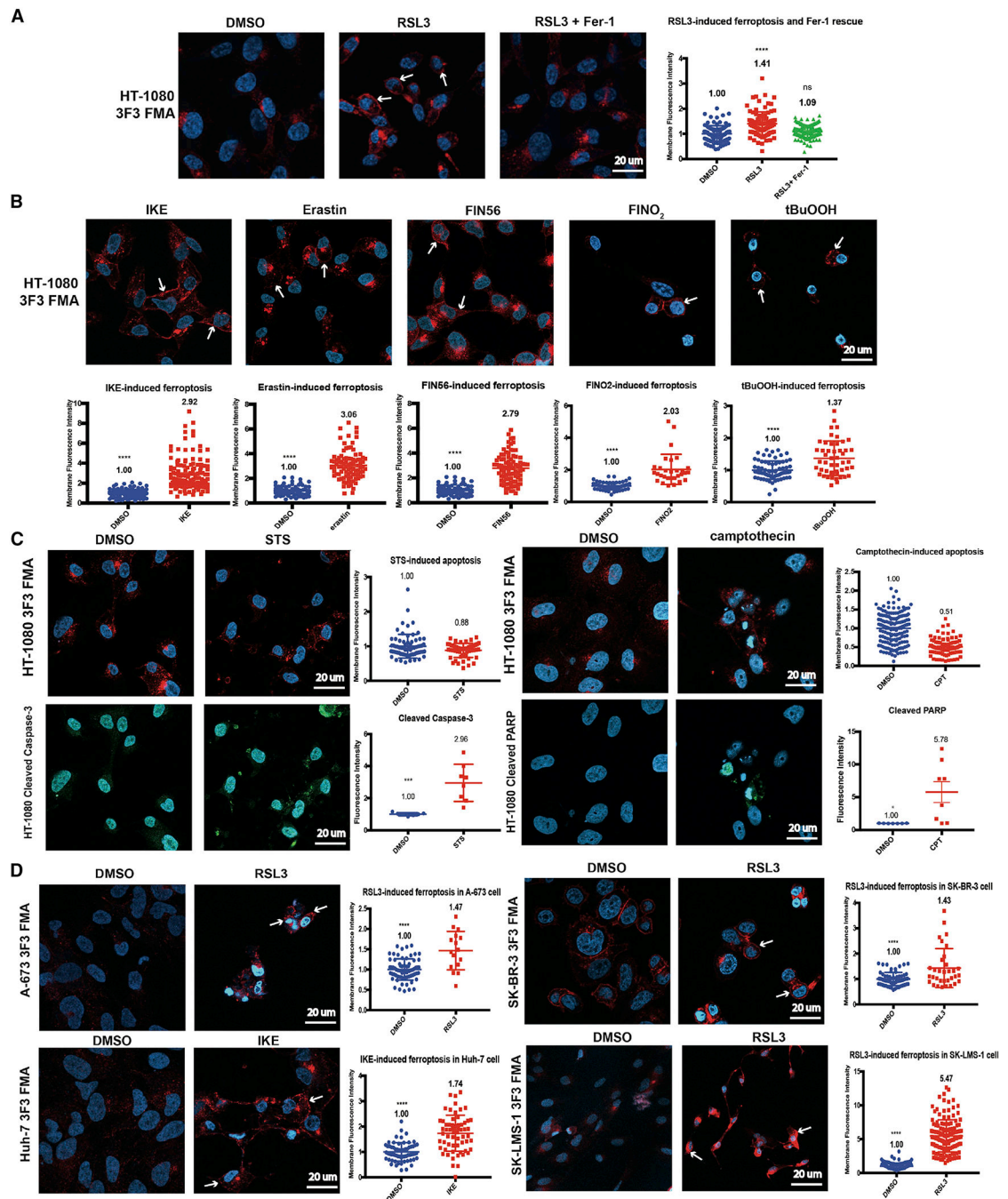
See also Figure S1.

Figure 2. Identification of 3F3-FMA as a Ferroptosis Marker Using Various Cell Death Inducers and Different Cell Lines

(A) HT-1080 cells (human fibrosarcoma cells) were incubated with 1 μM RSL3 or 1 μM RSL3 + 5 μM Fer-1 for 4 h. 3F3-FMA showed a significantly different pattern upon RSL3-induced ferroptosis, but not with fer-1 co-treatment. Nuclei were stained with DAPI (blue). 3F3-FMA was stained with Alexa Fluor 594 (red). White arrows indicate the differences. The quantification of membrane intensities of 3F3-FMA is shown at right (DMSO n = 107; RSL3 n = 96; RSL3 + Fer-1 n = 123). ****p 0.0001, ns, p > 0.05 (one-way ANOVA). Data plotted are mean ± SEM. Each dot represents 1 cell.

(B) HT-1080 cells (human fibrosarcoma cells) were incubated with 10 μM IKE for 8 h, 15 μM erastin for 8 h, 10 μM FIN56 for 8 h, 15 μM FINO$_2$ for 8 h, and 100 μM tBuOOH for 8 h. 3F3-FMA showed a reproducible staining pattern upon IKE-induced, erastin-induced, FIN56-induced, FINO2-induced, and tBuOOH-induced ferroptosis. Nuclei were stained with DAPI (blue). 3F3-FMA was stained with Alexa Fluor 594 (red). White arrows indicate the differences. The quantification of membrane intensities of 3F3-FMA is shown at bottom (IKE n = 113 and 129; erastin n = 68 and 92; FIN56 n = 68 and 86; FINO2 n = 59 and 30; tBuOOH n = 73 and 49). ****p   0.0001 (2-tailed t test). Data plotted are mean ± SEM. Each dot represents 1 cell.

(C) HT-1080 cells (human fibrosarcoma cells) were incubated with 1 μM staurosporine (STS) for 6 h and 2 μM camptothecin for 24 h. Cleaved caspase-3 antibody and cleaved PARP antibody were used to mark the induction of apoptosis. The staining pattern of 3F3-FMA during apoptosis was different from ferroptosis. Nuclei were stained with DAPI (blue). 3F3-FMA was stained with Alexa Fluor 594 (red). The quantification of membrane intensity of 3F3-FMA (DMSO n = 71; STS n = 53; DMSO n = 166; camptothecin n = 91) and overall intensity of cleaved caspase-3 (n = 7) and cleaved PARP (n = 7) is shown at right. *p   0.05, ***p   0.001. Data plotted are mean ± SEM. Each dot represents 1 cell.

(D) A-673 cells, SK-BR-3 cells, Huh-7 cells, and SK-LMS-1 cells were incubated with 1 μM RSL3 for 4 h. The same pattern as with 3F3-FMA was observed. Nuclei were stained with DAPI (blue). 3F3-FMA was stained with Alexa Fluor 594 (red). White arrows indicate the differences. The quantification of membrane intensities of 3F3-FMA is shown at right (A-673 n = 70 and 16; SK-BR-3 n = 65 and 33; Huh-7 n = 63 and 61; SK-LMS-1 n = 149 and 139). ****p   0.0001 (2-tailed t test). Data plotted are mean ± SEM. Each dot represents 1 cell.
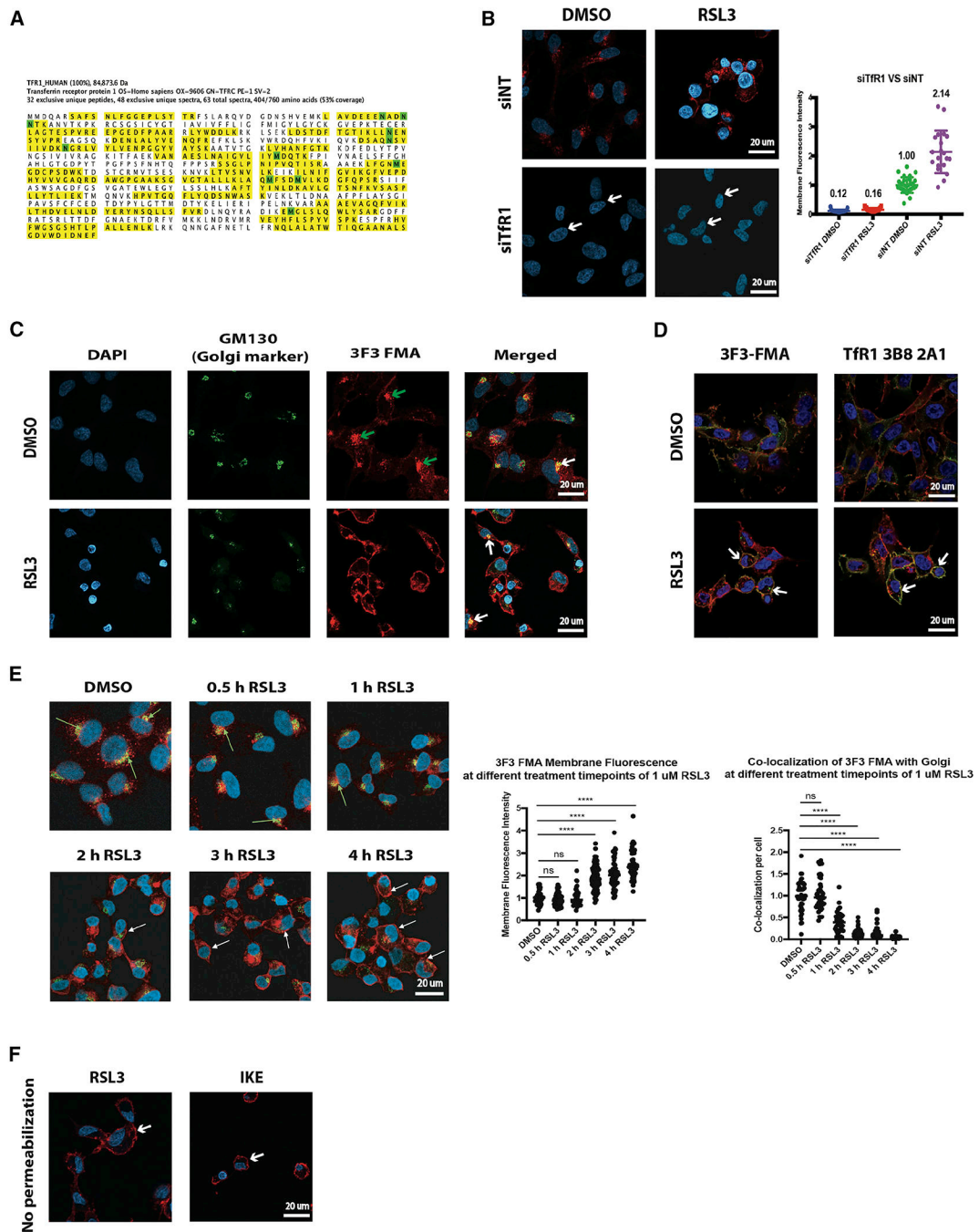
See also Figure S2.

Figure 3. The Target of 3F3-FMA Is TfR1, Which Is Located in the Golgi and the Plasma Membrane

(A) IP-mass spectrometry (MS) result of human TfR1 sequence. Yellow represents the identified sequences. Green indicates modified amino acids (M, oxidation of methionine; N, deamination of asparagine). The sequence coverage was 53%.

(B) siTfR1 or siNT 10 μM were combined with lipofectamine RNAiMAX in Opti-Mem media for 48 h. Then, HT-1080 cells were re-seeded in regular medium for an additional 24 h. Cells were incubated with 1 μM RSL3 for 4 h and then were fixed, permeabilized, and stained for DAPI (nuclei, blue) and 3F3-FMA (red). No 3F3-FMA was detected upon

siRNA knockdown of transferrin receptor. siNT was used as a control. The white arrows indicate absence.

(C) HT-1080 cells were incubated with 1 μM RSL3 for 4 h and then were fixed, permeabilized, and stained with DAPI (nuclei, blue), GM130 (Golgi, green), and 3F3-FMA. 3F3-FMA co-localized with the Golgi complex. The white arrows indicate overlap. The green arrows indicate the bright dots of 3F3-FMA in normal conditions.

(D) HT-1080 cells were incubated with 1 μM RSL3 for 4 h and then were fixed and stained with DAPI (nuclei, blue), WGA (plasma membrane, red), and 3F3-FMA or TfR1 3B8 2A1 (green). 3F3-FMA and TfR1 3B8 2A1 co-localized with the plasma membrane during RSL3-induced ferroptosis. The white arrows indicate the overlap.

(E) HT-1080 cells were incubated with 1 μM RSL3 for 4 h and collected at 0-, 0.5-, 1-, 2-, 3-, and 4-h time points. Cells were then fixed, permeabilized, and stained with DAPI (nuclei, blue), GM130 (Golgi, green), and 3F3-FMA. The white arrows indicate the accumulation of TfR1 in the plasma membrane, while the green arrows indicate the overlap area with the Golgi region. More membrane-located TfR1 and less Golgi-region-located TfR1 were observed. The quantification of membrane intensities of 3F3-FMA and co-localization of the Golgi marker GM130 and 3F3-FMA are shown at bottom. ****p   0.0001; ns, p > 0.05 (2-tailed t test). Data plotted are mean ± SEM. Each dot represents 1 cell.

(F) HT-1080 cells were incubated with 1 μM RSL3 for 4 h or 5 μM IKE for 18 h and then were fixed and stained with DAPI (nuclei, blue) and 3F3-FMA (red). Without permeabilization, 3F3-FMA stained the cell surface clearly for cells undergoing ferroptosis. The white arrows indicate the boundaries.
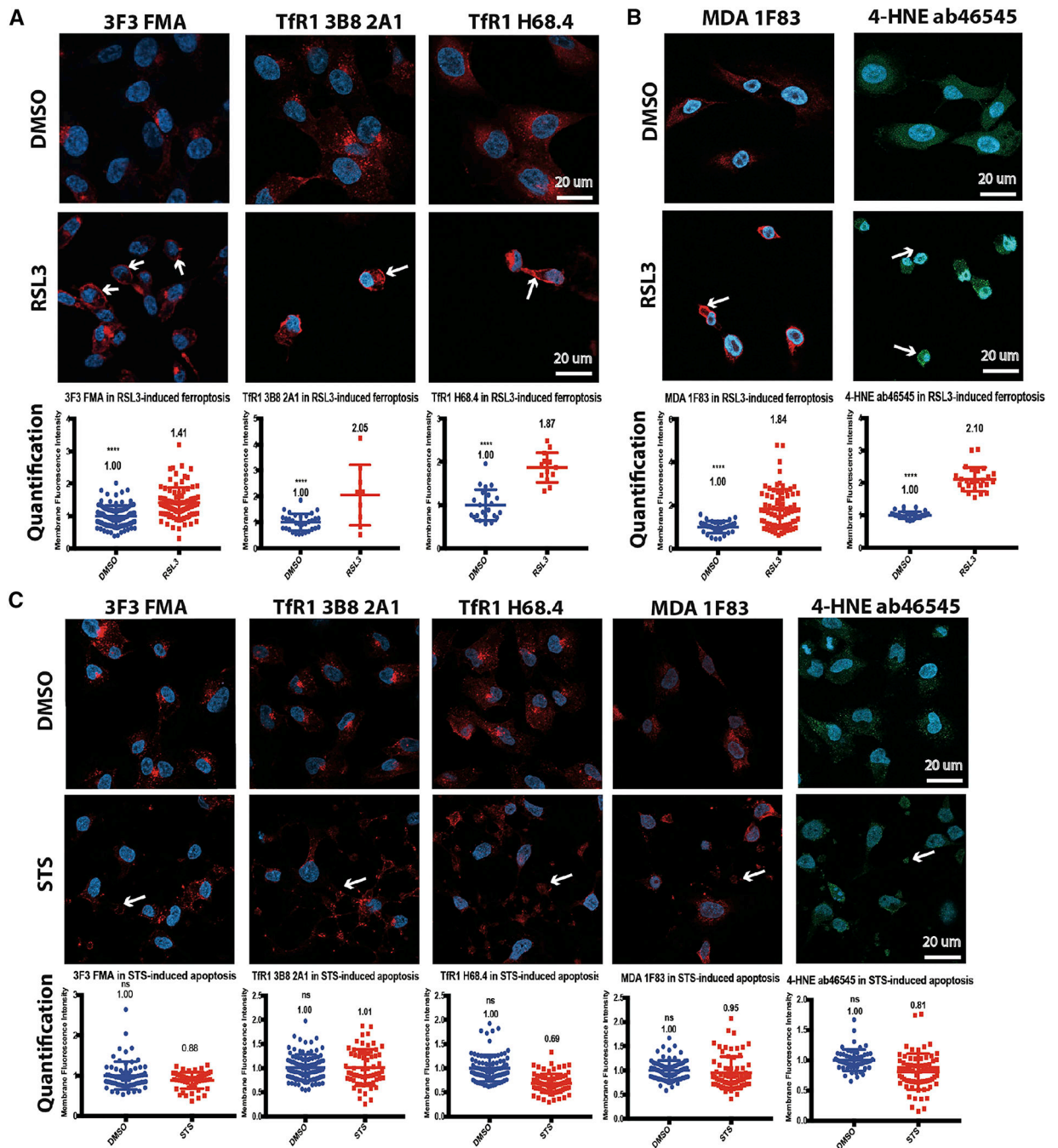
See also Figure S3.

Figure 4. 3F3-FMA, Anti-TfR1 3B8 2A1, Anti-TfR1 H68.4, Anti-MDA 1F83, and Anti-4-HNE Antibodies Can Be Used as Ferroptosis Markers by Immunofluorescence

(A) HT-1080 cells were incubated with 1 μM RSL3 for 4 h and then were fixed, permeabilized, and stained with DAPI (nuclei, blue), 3F3-FMA, anti-TfR1 3B8 2A1, or anti-TfR1 H68.4 antibodies (red). The white arrows indicate differences. The quantification of membrane intensities of anti-TfR1 antibodies is shown at bottom (3F3-FMA n = 107 and 96; TfR1 3B8 2A1 n = 32 and 9; TfR1 H68.4 n = 22 and 13). ****p 0.0001 (2-tailed t test). Data plotted are mean ± SEM. Each dot represents 1 cell.

(B) HT-1080 cells were incubated with 1 μM RSL3 for 4 h and then were fixed, permeabilized, and stained with DAPI (nuclei, blue), anti-MDA 1F83 antibody (red), and anti-4-HNE ab46545 antibodies (green). The white arrows indicate differences. The quantification of membrane intensities of the antibodies is shown at bottom (MDA 1F83 n = 35 and 73; 4-HNE ab46545 n = 33 and 26). ****p   0.0001 (2-tailed t test). Data plotted are mean ± SEM. Each dot represents 1 cell.

(C) HT-1080 cells were incubated with 1 μM STS for 6 h and then were fixed, permeabilized, and stained with DAPI (nuclei, blue), 3F3-FMA (red), anti-TfR1 3B8 2A1 (red), anti-TfR1 H68.4 (red), anti-MDA 1F83 (red), and anti-4-HNE ab46545 antibodies (green). The white arrows indicate the stain outside intact cells. The quantification of membrane intensities of the antibodies is shown at bottom (3F3-FMA n = 71 and 53; TfR1 3B8 2A1 n = 103 and 63; TfR1 H68.4 n = 93 and 80; MDA 1F83 n = 81 and 71; 4-HNE ab46545 n = 56 and 69). ns, p > 0.05 (2-tailed t test). Data plotted are mean ± SEM. Each dot represents 1 cell.
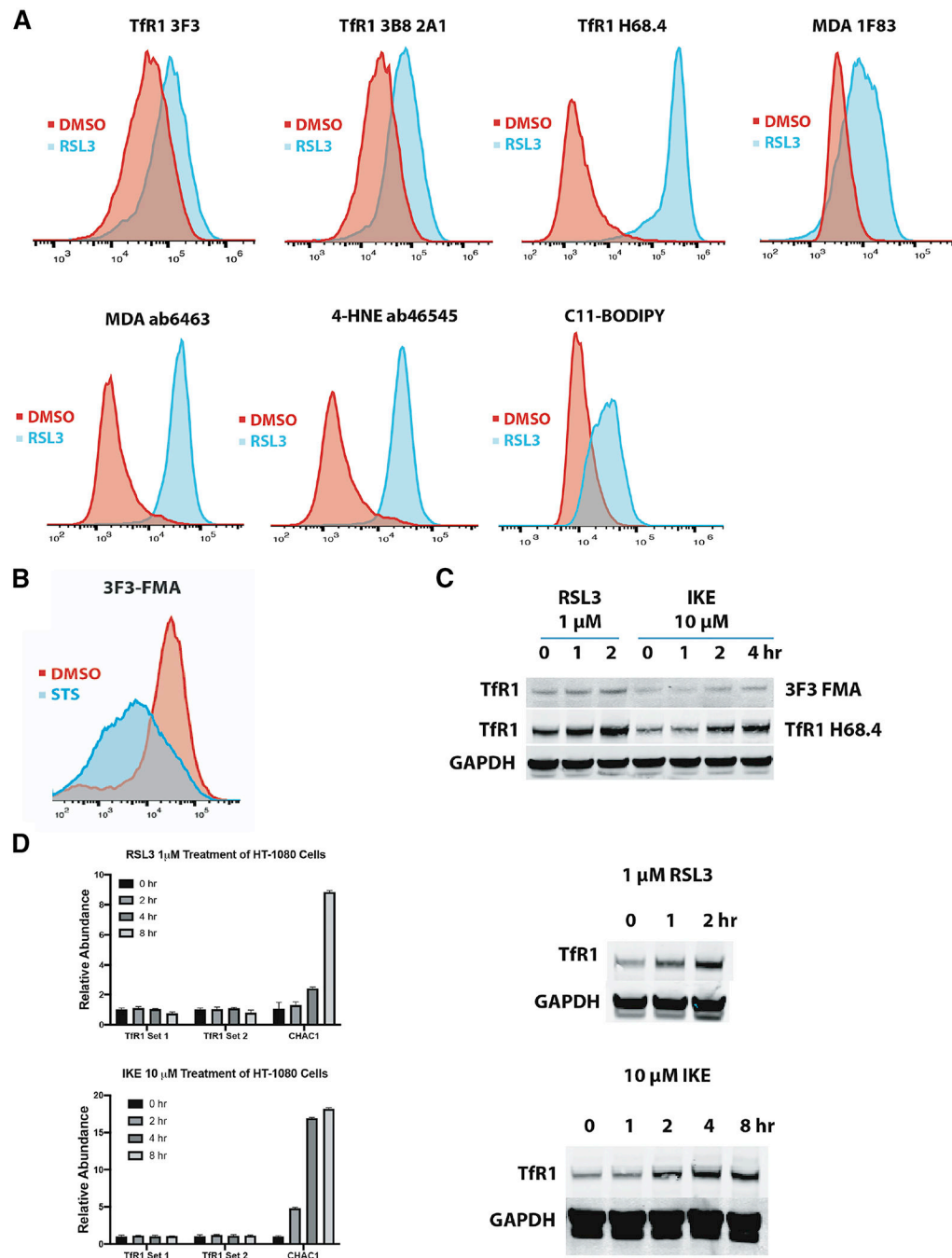
See also Figure S4.

Figure 5. Anti-TfR1, Anti-MDA, and Anti-4-HNE Antibodies Were Effective in Flow Cytometry Applications, While 3F3-FMA and TfR1 H68.4 Antibodies Were Effective in Western Blot Applications

(A) HT-1080 cells were treated with DMSO or 1 μM RSL3 for 4 h. Cells were then harvested and stained with 1st and 2nd antibodies or C11-BODIPY without permeabilization. Approximately 15,000 cells were recorded and gated. RSL3-treated cells had increased intensities for 3F3-FMA, TfR1 3B8 2A1, TfR1 H68.4, MDA 1F83, MDA ab6463, and 4-HNE ab46545. C11-BODIPY, a probe for lipid peroxidation was used as a metric.

(B) HT-1080 cells were treated with DMSO or 1 μM STS for 6 h. Cells were then harvested and stained with 1st and 2nd antibodies without permeabilization. Approximately 50,000 cells were recorded and gated. STS-treated cells had decreased intensities of 3F3-FMA staining.

(C) HT-1080 cells were treated with 1 μM RSL3 for 2 h and 10 μM IKE for 4 h. Cells were collected at multiple time points, as shown. Cells were then lysed, stained with 1st and 2nd antibodies, and detected using western blot. 3F3-FMA and TfR1 H68.4 were used as TfR1 antibodies. An increased amount of TfR1 protein was observed during ferroptosis. GAPDH was used as a control.

(D) HT-1080 cells were treated with 1 μM RSL3 or 10 μM IKE for 8 h. cDNAs were generated from total RNA collected and purified from cells. Two sets of TfR1 primers were used to quantify the amount of cellular TfR1 transcripts. CHAC1 was used as a positive control. The level of TfR1 mRNAs did not increase during ferroptosis. Blotting of TfR1 proteins using TfR1 H68.4 antibody is shown side by side. RSL3-treated western blot, 4 and 8 h, were not harvested due to an insufficient number of viable cells.
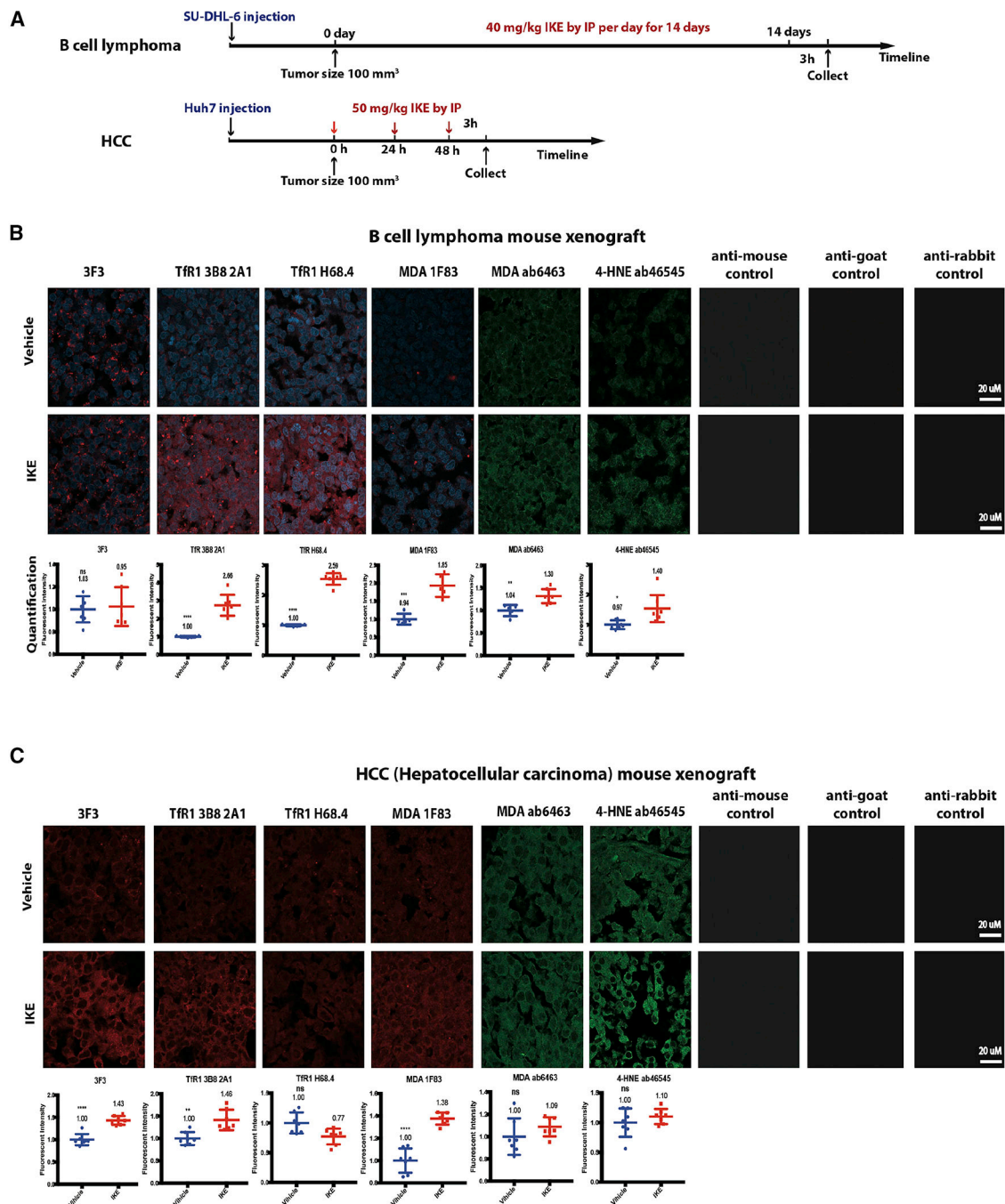
Figure 6. Comparison of TfR1 Antibodies and Other Potential Ferroptosis-Staining Reagents in Mouse Xenograft Tumor Tissue Samples

(A) An illustration of the preparation of the mouse xenograft tumor and IKE dose.

(B) B cell lymphoma tumor tissues were fixed in 4% paraformaldehyde (PFA) for 24 h, perfused in 30% sucrose for 24 h, and stained with 1st and 2nd antibodies. Anti-TfR1 3B8 2A1, anti-TfR1 H68.4, and anti-MDA 1F83 showed a significant difference in intensities between vehicle and IKE treatments, 3F3-FMA showed no difference, and anti-MDA ab6463 and anti-4-HNE ab46545 showed slight differences. Controls without primary antibody staining are shown at right. The quantification of overall intensity of the antibodies

is shown at bottom (n = 7). ****p 0.0001, ***p 0.001, **p 0.01, *p 0.05, and ns, p > 0.05 (2-tailed t test). Data plotted are mean ± SEM. Each dot represents 1 image.

(C) HCC tumor tissues was fixed in 4% PFA for 24 h, perfused in 30% sucrose for 24 h, and stained with 1st and 2nd antibodies. 3F3-FMA, anti-TfR1 3B8 2A1, and anti-MDA 1F83 showed differences in intensities between vehicle and IKE groups, while other antibodies did not. Controls without primary antibody staining are shown at right. The quantification of overall intensity of the antibodies is shown at bottom (n = 7). ****p 0.0001, **p 0.01, and ns, p > 0.05 (2-tailed t test). Data plotted are mean ± SEM. Each dot represents 1 image. See also Figure S6.

Table 1.

Summary of Different Results for All Antibodies

Application	Antibody							
	3F3-FMA	TfR1 3B8 2A1	TfR1 H68.4	TfR1 D7G9X	MDA 1F83	MDA ab6463	4-HNE ab46545	ACSL4 sc-365230
IF in cell culture	✔	✔	✔	X	✔	X	✔	X
Flow cytometry	✔	✔	✔	NA	✔	✔	✔	NA
Lymphoma tissue	X	✔	✔	NA	✔	✔	✔	NA
HCC tissue	✔	✔	✔	NA	✔	X	X	NA

Eight antibodies were evaluated in cell culture IF (immunofluorescence), flow cytometry, and two mouse xenograft tumor tissue samples by immunofluorescence. Anti-TfR1 3B8 2A1 and anti-MDA 1F83 performed well in all of the samples.

KEY RESOURCES TABLE

REAGENT or RESOURCE	SOURCE	IDENTIFIER
Antibodies		
3F3-FMA	This paper	N/A
Anti-dihydropyridine-MDA-lysine adduct mouse mAb 1F83	Reference (Yamada et al., 2001)	N/A
Transferrin Receptor/CD71 Monoclonal Antibody, Clone: H68.4, Invitrogen	Thermo Fisher Scientific	Cat#13–6800, RRID:AB_2533029
Cd71 (D7G9X) XP® Rabbit mAb	Cell Signaling Technology	Cat#13113, RRID:AB_2715594
CD71 (3B8 2A1)	Santa Cruz Biotechnology	Cat#sc-32272, RRID:AB_627167
Tom20 (FL-145)	Santa Cruz Biotechnology	Cat#sc-11415, RRID:AB_2207533
PDI antibody [RL90] - ER Marker	Abcam	Cat#ab2792, RRID:AB_303304
Gm130 (D6B1) XP® Rabbit mAb	Cell Signaling Technology	Cat#12480, RRID:AB_2797933
Anti-malondialdehyde antibody	Abcam	Cat#ab6463, RRID:AB_305484
Anti-4-hydroxynonenal antibody	Abcam	Cat#ab46544, RRID:AB_722493
Anti-ACSL4 antibody (F-4)	Santa Cruz Biotechnology	Cat# sc-365230, RRID:AB_10843105
Goat anti-Mouse IgG (H+L) Highly Cross-Adsorbed Secondary Antibody, Alexa Fluor 594	Thermo Fisher Scientific	Cat#A-11032, RRID:AB_2534091
Goat anti-Rabbit IgG (H+L) Highly Cross-Adsorbed Secondary Antibody, Alexa Fluor 488	Thermo Fisher Scientific	Cat#A-11034, RRID:AB_2576217
EGFR Monoclonal Antibody (H11)	Thermo Fisher Scientific	Cat# MA5–13070, RRID:AB_10977527
CD20	Abcam	Cat#ab194970
Glypican 3 Polyclonal Antibody	Thermo Fisher Scientific	Cat# PA5–47256, RRID:AB_2608607
CD8a (D8A8Y) Rabbit mAb antibody	Cell Signaling Technology	Cat# 85336, RRID:AB_2800052
CD45 (D9M8I) XP antibody	Cell Signaling Technology	Cat# 13917, RRID:AB_2750898
Cleaved Caspase-3 (Asp175) Antibody	Cell Signaling Technology	Cat# 9661, RRID:AB_2341188
Cleaved PARP (Asp214) (D64E10) XP® Rabbit mAb	Cell Signaling Technology	Cat# 5625, RRID:AB_10699459
Biological Samples		
B cell lymphoma mouse xenograft model	Reference (Zhang et al., 2019)	N/A
Hepatocellular carcinoma (HCC) mouse xenograft model	Brent R. Stockwell lab	N/A
Murine glioma model	Peter D. Canoll lab	N/A
Chemicals, Peptides, and Recombinant Proteins		
RSL3	Reference (Yang and Stockwell, 2008)	N/A
Imidazole ketone erastin (IKE)	Reference (Larraufie et al., 2015)	N/A
Erastin	Reference(Dolma et al., 2003)	N/A
FIN56	Reference(Shimada et al., 2016)	N/A
FINO$_2$	Reference(Gaschler et al., 2018)	N/A
Staurosporine (STS)	Selleck Chemicals	Cat#S1421
Ferrostatin-1 (Fer-1)	Reference(Skouta et al., 2014)	N/A

REAGENT or RESOURCE	SOURCE	IDENTIFIER
C11-BODIPY(BODIPY 581/591 C11)	Thermo Fisher Scientific	Cat#D3861
Critical Commercial Assays		
Plasma Membrane Protein Extraction Kit	Abcam	Cat#ab65400
Deposited Data		
Mass Spec data of TfR1	This paper	PXD017425; http://proteomecentral.proteomexchange.org
Experimental Models: Cell Lines		
OCI-LY7	DSMZ	Cat# ACC-688, RRID:CVCL_1881
HT-1080	ATCC	Cat# CRL-7951, RRID:CVCL_0317
A-673	This lab	N/A
SK-BR-3	This lab	N/A
SK-LMS-1	This lab	N/A
Huh-7	This lab	N/A
Oligonucleotides		
SMARTpool: ON-TARGETplus TFRC siRNA	Dharmacon	Cat# L-003941-00-0005 5 nmol
qPCR primers targeting TfR1 FWD: ACCATTGTCATATACCCGGTTCA	This paper	N/A
qPCR primers targeting TFR1 RV: CAATAGCCCAAGTAGCCAATCAT	This paper	N/A
qPCR primers targeting GAPDH FWD: CTCCAAAATCAAGTGGGGCG	This paper	N/A
qPCR primers targeting GAPDH RV: ATGACGAACATGGGGGCATC	This paper	N/A
Software and Algorithms		
Columbus Software 2.8.0	PerkinElmer	https://www.perkinelmer.com
CellProfiler 3.1.8	CellProfiler Image Analysis Software	https://cellprofiler.org
Prism, Version 7.0	GraphPad Software	https://www.graphpad.com/scientific-software/prism/
MaxQuant v.1.6.1.0	MaxQuant	https://www.maxquant.org/
Other		
ProLong Diamond antifade mountant with DAPI	ThermoFisher	Cat#P36962
RIPA buffer	Thomas Scientific	Cat#89900
10% goat serum	Thermo Fisher Scientific	Cat#50197Z